Acta Neuropathologica (2024) 147:72
https://doi.org/10.1007/s00401-024-02726-w

ORIGINAL PAPER

Characterization of *NEB* pathogenic variants in patients reveals novel nemaline myopathy disease mechanisms and omecamtiv mecarbil force effects

Esmat Karimi[1] · Jochen Gohlke[1] · Mila van der Borgh[1] · Johan Lindqvist[1] · Zaynab Hourani[1] · Justin Kolb[1] · Stacy Cossette[2] · Michael W. Lawlor[2,3] · Coen Ottenheijm[1,4] · Henk Granzier[1]

Received: 22 December 2023 / Revised: 19 March 2024 / Accepted: 26 March 2024

Abstract

Nebulin, a critical protein of the skeletal muscle thin filament, plays important roles in physiological processes such as regulating thin filament length (TFL), cross-bridge cycling, and myofibril alignment. Pathogenic variants in the nebulin gene (*NEB*) cause NEB-based nemaline myopathy (NEM2), a genetically heterogeneous disorder characterized by hypotonia and muscle weakness, currently lacking curative therapies. In this study, we examined a cohort of ten NEM2 patients, each with unique pathogenic variants, aiming to understand their impact on mRNA, protein, and functional levels. Results show that pathogenic truncation variants affect *NEB* mRNA stability and lead to nonsense-mediated decay of the mutated transcript. Moreover, a high incidence of cryptic splice site activation was found in patients with pathogenic splicing variants that are expected to disrupt the actin-binding sites of nebulin. Determination of protein levels revealed patients with either relatively normal or markedly reduced nebulin. We observed a positive relation between the reduction in nebulin and a reduction in TFL, or reduction in tension (both maximal and submaximal tension). Interestingly, our study revealed a pathogenic duplication variant in nebulin that resulted in a four-copy gain in the triplicate region of NEB and a much larger nebulin protein and longer TFL. Additionally, we investigated the effect of Omecamtiv mecarbil (OM), a small-molecule activator of cardiac myosin, on force production of type 1 muscle fibers of NEM2 patients. OM treatment substantially increased submaximal tension across all NEM2 patients ranging from 87 to 318%, with the largest effects in patients with the lowest level of nebulin. In summary, this study indicates that post-transcriptional or post-translational mechanisms regulate nebulin expression. Moreover, we propose that the pathomechanism of NEM2 involves not only shortened but also elongated thin filaments, along with the disruption of actin-binding sites resulting from pathogenic splicing variants. Significantly, our findings highlight the potential of OM treatment to improve skeletal muscle function in NEM2 patients, especially those with large reductions in nebulin levels.

Keywords Nemaline myopathy · Nebulin · Omecamtiv mecarbil · Cyptic splice-site

Introduction

Nemaline myopathy (NEM) is a rare, clinically and genetically heterogeneous disorder [54], characterized by hypotonia and muscle weakness [91]. NEM is histopathologically defined by disorganization of the sarcomeric Z discs and the accumulation of nemaline bodies or rods in muscle fibers, which are aggregates of Z-disc and thin filament proteins [94]. Moreover, NEM patients exhibit a shift towards type 1 fibers, a characteristic evident in both patient samples and mouse models of NEM [58, 69]. Studies indicate an estimated incidence of two cases per 100,000 live births, accounting for 17% of congenital myopathy cases [72]. The

✉ Henk Granzier
granzier@arizona.edu

1 Department of Cellular and Molecular Medicine, University of Arizona, Tucson, AZ, USA

2 Department of Pathology, Medical College of Wisconsin, Milwaukee, WI, USA

3 Diverge Translational Science Laboratory, Milwaukee, WI, USA

4 Department of Physiology, Amsterdam UMC (Location VUMC), Amsterdam, Netherlands

Published online: 18 April 2024

muscle weakness ranges from severe to mild [73, 74, 92, 93, 95], and is most commonly congenital [1, 96].

Nemaline myopathies are associated with pathogenic variants in at least 13 genes: *ACTA1*, *NEB*, *LMOD3*, *TPM3*, *TPM2*, *TNNT1*, *TNNT3*, *CFL2*, *MYPN* (all encoding protein components of the muscle thin filament), *KBTBD13*, *KLHL40*, *KLHL41* (all likely involved in protein turnover in the muscle sarcomere via the ubiquitin–proteasome pathway), and *MYO18B* [54, 85]. These pathogenic variants can be either de novo, or inherited by autosomal dominant, or autosomal recessive patterns [54]. Pathogenic variants in the *NEB* gene account for approximately 35% of nemaline myopathies [57], which are usually inherited recessively. However, a recent study identified the first dominantly inherited pathogenic variant in *NEB*, leading to a distal form of nemaline myopathy [33].

Nebulin, a giant ~ 800 KDa filamentous protein, is a crucial component of the thin filament in skeletal muscle [37]. Single nebulin molecules span the thin filament, with their C-termini anchored in the Z-disk and N-terminal directed toward the pointed-end of the thin filament [60]. In human muscle, nebulin primarily consists of 22 to 29 tandem super-repeats (SR) [19, 65, 105]. Each SR consists of seven simple repeats, each comprised of 31 to 38 amino acid residues, featuring a conserved sequence motif SDxxYK that is thought to be actin binding [97]. Every nebulin simple repeat interacts with three neighboring actin subunits [97]. Nebulin's SRs interact with the troponin/tropomyosin regulatory complex via two contact sites between troponin T and nebulin, facilitated by troponin-binding motifs, including WLKGIGW and ExxK [97]. Nebulin plays a critical role in various important processes in skeletal muscle such as maintaining Z-disk structure, myofibril alignment [2, 10, 87] and crossbridge cycling [3, 8, 40, 59, 61, 62]. It has also been implicated in the regulation of thin filament length (TFL), as reduced levels of nebulin protein have been associated with shortened TFL in patients with NEB-related nemaline myopathy, as well as in nebulin-deficient mouse models, zebrafish, and chick skeletal myocytes [3, 36, 43, 61, 63, 64, 83, 102, 103].

Despite investigating a number of therapeutic interventions including troponin activators such as Levosimendan [14], CK-20066260 [61], dietary supplements [81] and myostatin inhibitors [47, 84], there are currently no effective therapies targeting the underlying pathological mechanisms for nebulin-based NEM (NEM2). It has been shown that Omecamtiv mecarbil (OM), a selective small-molecule activator of cardiac myosin (*MYH7)* that was initially developed as a treatment for heart failure [67, 82], increases submaximal force production in type 1 skeletal muscles of Neb cKO mouse model [48] and rat diaphragm [56]. Considering the dominance of type 1 fibers in nemaline myopathy patients [58, 69], it is expected that OM increases the force of type 1 fibers at submaximal activation levels in skeletal muscle fibers and so might improve the quality of life in nemaline myopathy patients.

Here, we studied skeletal muscle tissue from a cohort of ten NEM2 patients with confirmed pathogenic or VUS variants in the *NEB* gene. We characterized these variants by studying their effects on mRNA and protein levels as well as mechanical features of skeletal muscle. Our results revealed novel NEM disease mechanisms including disruption of actin binding sites by activation of cryptic splice sites. Furthermore, we showed that OM not only improves force production in slow skeletal muscle at submaximal activation levels, but that its effectiveness is greater in NEM2 patients relative to controls, with an inverse relation between nebulin level and OM-based tension increase.

Materials and methods

Skeletal muscle biopsies of NEM2 patients

Surgically obtained muscle biopsy samples of NEM2 patients, from thigh, triceps or paraspinal were obtained from Congenital Muscle Disease Tissue Repository (CMD-TR) housed at the Medical College of Wisconsin, along with limited data including their NEB variants. We also obtained control biopsy samples from vastus lateralis muscles of 34 years old healthy individuals from the University of Montana [66]. The subjects' consent was obtained according to the Declaration of Helsinki and ethical approval for study of human biopsies was granted by Institutional Review Board of University of Arizona. All biopsies were stored frozen and unfixed at −80 °C until use.

RNAseq analysis

Around 15–150 mg (depending on quality of biopsy) of frozen muscle tissue from NEM2 or control biopsy samples were collected and stored in RNAlater to reserve RNA integrity. For RNA extraction, 600 µl of prechilled buffer RLT (RNeasy Fibrous Tissue Mini Kit, Qiagen) with 1% β-mercaptoethanol was added to muscle tissue stored in RNAlater in a 4-ml cryovial. Tissue was disrupted using a rotor–stator homogenizer for 30 s. RNA extraction was performed following the manufacturer's instructions and quantified using a Nanodrop ND-1000 spectrophotometer (Thermo Fisher Scientific). RNA integrity was checked on a 2100 Bioanalyzer (Agilent), and all RNA integrity number scores were confirmed to be ≥ 8.

For library preparation, ribosomal RNA (rRNA) was depleted from RNA preparations with a NEBnext rRNA depletion kit using 1 µg of total RNA as starting material. Libraries were prepared using the NEBNext Ultra II

Directional RNA Library Prep Kit for Illumina following the manufacturer's instructions. RNA was fragmented for 10 min at 94 °C. For first strand cDNA synthesis, incubations were for 10 min at 25 °C followed by 50 min at 42 °C and 15 min at 70 °C. For size selection, conditions for an approximate insert size of 300 bp were used. Size-selected libraries were enriched by PCR for 10 cycles and purified using NEBnext sample purification beads. Library quality and insert sizes were checked using a 2100 Bioanalyzer (Agilent). Sequencing was performed on an Illumina Hiseq2500 sequencer using 150-bp paired-end sequencing. The raw data are available (BioProject accession PRJNA996928). Adapters and low quality reads were removed with Trim Galore (www.bioinformatics.babraham.ac.uk/projects/trimgalore/), and reads were mapped to the human genome (Release GRCh38.p13) using STAR [17] with default settings.

For calculating inclusion percentages of all exons from nebulin transcripts, inclusion reads (IRs) and exclusion reads (ERs) were counted for each exon based on nebulin isoform NM_001271208. IRs are reads overlapping the exon being investigated, normalized by exon length. ERs are reads either upstream or downstream that support exclusions of the read. From these factors, the following equations were used to calculate the PSI index using the ASpli R-package [51]

$$IR_{i,n} = IR_i/\text{length exon}_i + \text{read length} - 1$$

$$ER_{i,n} = ER_i/\text{read length} - 1$$

$$PSI_i = \left(IR_{i,n}/IR_{i,n} + ER_{i,n}\right)$$

where i is the exon number and n is the normalized read counts.

Read density (normalized reads per base) was calculated by dividing read counts (per exon) by exon length. Read density was then divided by mean density in control samples. To estimate the number of added TRI repeats in patient 180, normalized read density was then multiplied by exon length and exon length was subtracted to estimate the number of additional bases per exon (Supplementary Table 3). The estimated number of added bases was then divided by the average repeat length to estimate the number of additional (super)-repeats.

For detection of alternative splicing events around the splicing variants, the most frequent events were considered, and junction reads were used to calculate relative frequencies of events (exon skipping vs. intron inclusion vs. normal junction usage).

For allelic ratio calculations, base composition at single genomic positions was determined using the mpileup function from samtools [11]. Alleles at mutated positions were counted and ratios were calculated as follows: Allele 1 (mutated) / (Allele 1 (mutated) + Allele 2 (wt)). Following this calculation, equal expression from both alleles would give a ratio of 0.5. Degradation of the mutated allele by NMD would shift the ratio closer to zero and result in allelic imbalance.

Structure prediction with AlphaFold/colabfold

Alpha-helical portions of nebulin were predicted with Colabfold [53] using standard settings. As inputs for structure predictions, sequence lengths of two super-repeats around in-frame intron inclusions were selected (super-repeats 3–4 for patient 4001 and super-repeats 15–16 for patient 2622).

Omecamtive mecarbil

Omecamtiv mecarbil (OM) was purchased from Selleckchem (Houston, TX) and was dissolved in dimethylsulfoxide (DMSO) to make a stock solution as instructed by the manufacturer. OM stock solution was then added to the experimental solution to prepare the final desired concentration of OM. while keeping the concentration of DMSO at 0.5%. Based on our previous study that showed the force increase with OM reached a plateau between 0.5 and 1.0 µM, and with force starting to decrease at higher concentrations, we used 0.5 µM OM here [48]. 0.5% DMSO was used as vehicle.

Skeletal muscle mechanics

Small pieces cut from the frozen muscle biopsies were placed in 50% glycerol/relaxing solution (in mM: 40 BES, 10 EGTA, 6.56 MgCl2, 5.88 NaATP, 1 DTT, 46.35 K-propionate, 15 creatine phosphate, Ionic strength 180 mM, pH 7.0 at 20 °C) containing protease inhibitors (in mM: 0.01 E64, 0.04 leupeptin and 0.5 PMSF) and stored overnight at −20 °C. The solution was replaced with fresh 50% glycerol/relaxing solution the following day and the muscle tissue was membrane-permeabilized at 4 °C overnight as described previously [24]. This procedure renders the membranous structures in the muscle fibers permeable, which enables activation of the myofilaments with exogenous calcium. Preparations were washed thoroughly with relaxing solution and stored in 50% glycerol/relaxing solution at −20 °C. Muscles were used for experiments within 1 week. Small muscle bundles or single muscle fibers were dissected from the permeabilized strips and were mounted between a length motor (ASI 403A, Aurora Scientific Inc., Ontario, Canada) and a force transducer element (ASI 315C-I, Aurora Scientific Inc., Ontario, Canada) in a single fiber apparatus (ASI 802D, Aurora Scientific Inc., Ontario, Canada)

that was mounted on the stage of an inverted microscope (Zeiss Axio Observer A1, Zeiss, Thornwood, NY, USA). Sarcomere length was set using a high-speed VSL camera and ASI 900B software (Aurora Scientific Inc., Ontario, Canada). Mechanical experiments were performed at a sarcomere length of 2.5 µm for all control and patients except patient 180 which we did mechanical experiments at sarcomere length of 2.7 µm. Fiber diameter and depth (determined with a build in prism that allowed for side view of the fiber) were measured at three points along the fiber, and the cross-sectional area was determined assuming an elliptical cross section. The temperature of the bathing solutions was kept constant at 20 °C using a TEC controller (ASI 825A, Aurora Scientific Inc. Ontario, Canada). After completion of the mechanical studies (below), fibers/bundles were fiber-typed. Other than relaxing solutions, we used pre-activation (in mM: 40 BES, 1 EGTA, 6.32 MgCl2, 5.82 NaATP, 1 DTT, 81.71 K-propionate, 15 creatine phosphate, pH 7.0 at 20˚C) and activation solution (in mM: 40 BES, 10 CaCO3 EGTA, 6.29 MgCl2, 6.12 Na-ATP, 1 DTT, 45.3 potassium-propionate, 15 creatine phosphate, Ionic strength 180 mM, pH 7.0 at 20˚C) to do following mechanical experiments.

Force-pCa relationship: To determine the effect of 0.5 µM OM on the force-pCa relation, permeabilized muscle fiber bundles or single fibers were sequentially bathed in a relaxing solution, a pre-activation solution, and activation solutions with pCa values ranging from 8.0 to 4–all containing 0.5 µM OM or vehicle–and the steady-state force was measured. The pCa-solutions were created by mixing relax and activating solutions taking into account the Kd of Ca^{2+} according to the model developed by Fabiato & Fabiato [21]. Measured force values were normalized to the maximal force obtained at pCa 4. The obtained force-pCa data were fit to the Hill equation ($Y = 1/(1 + 10nH(pCa - pCa50))$) where the pCa50 corresponds to the calcium concentration that yields half-maximal force and the Hill coefficient, nH, to myofilament cooperativity [80].

ktr-measurements: The rate of tension redevelopment (*ktr*) was measured at steady-state force by rapidly shortening (1 ms) the fiber at one end of the fiber resulting in unloaded shortening of the fiber for 20 ms. Remaining bound cross-bridges were detached by rapidly restretching the fiber to initial length and the tension redeveloped [4]. ktr was determined by fitting the rise of force to the following equation (one-phase association curve): $F = Fss * (1 - ektr * t) + c$, where F is force at time t, Fss is steady-state force (Supplementary Fig. 5a).

Step response protocol to measure dynamic stiffness: Muscle fibers were bathed in Ca^{2+} solutions (pCa6.75) with or without 0.5 µM OM treatment at 2.5 µm. Once the fiber preparations attained steady-state force, a series of rapid stretch and release length perturbations was applied (Supplementary Fig. 5b-Top) and then the various phases of the tension in response to muscle length (ML) changes (Supplementary Fig. 5b-bottom) were analyzed individually by fitting to a non-linear distortion recruitment (NLDR) model [52] to gain insights into cross-bridges mechanics (Ed, Er, b and c).

Myosin heavy chain composition

To determine the myosin isoform composition of muscle fibers that were used in mechanical experiments, we used Sodium dodecyl sulfate polyacrylamide gel electrophoresis as described previously [63]. In brief, after mechanical experiments, the single fibers or bundles were stored in SDS sample buffer containing 62.5 mM Tris_HCL, 2% (weight/volume) SDS, 10% (v/v) glycerol, and 0.001% (w/v) bromophenol blue at a pH of 6.8 and then were boiled for 3 min in 80°. The stacking gel contained a 4% acrylamide concentration (pH 6.7), and the separating gel contained 8% acrylamide (pH 8.7) with 30% glycerol (v/v). The gels were run for 24 h at 15 °C and a constant voltage of 275 V. Gels for whole muscle lysates were stained with Coomassie blue and single fiber gels were silver-stained. Gels were scanned and analyzed with ImageJ (v1.49, NIH, USA).

Sample preparation and gel electrophoresis

One part of the frozen biopsies was prepared as previously described [38, 99]. Briefly, the tissues were grinded to fine powder with glass pestles cooled in liquid nitrogen. The powder was primed were primed at −20 °C for a minimum of 20 min, then suspended in 50% urea buffer [(in mol/L) 8 urea, 2 thiourea, 0.05 Tris–HCl, 0.075 dithiothreitol with 3% SDS and 0.03% bromophenol blue pH 6.8] and 50% glycerol with protease inhibitors [(in mmol/L) 0.04 E64, 0.16 leupeptin and 0.2 PMSF] at 60 °C for 10 min. Then, the samples were centrifuged at 13 000 revolutions per minute (rpm) for 5 min, aliquoted and flash frozen in liquid nitrogen and stored at −80 °C. Nebulin was visualized by running the solubilized samples on 1.0% vertical SDS-agarose gel [38, 98] at 15 mA per gel for 3:20, staining the gel with coomassie blue, as described previously [38, 100] and scanning it using a commercial scanner. Nebulin quantification was done by analyzing the digitized gel patterns obtained by agarose gel electrophoresis. In our experience, it is not ideal to quantify proteins like nebulin via Western Blots because large proteins do not easily migrate out of the gel and the transfer is often incomplete. Hence, for quantification, it is desirable to analyze the protein gel directly, which is possible for nebulin as it is sufficiently abundant and does not overlap with other similarly sized proteins. The results shown in Fig. 3b, d were obtained by normalizing nebulin against MHC. To test whether this was appropriate we also normalized nebulin against all proteins that are smaller than MHC all the way

down to actin. Obtained results were indistinguishable from those that are shown in Fig. 3.

Western blots for nebulin were run with 0.8% agarose gels run for 15 mA/gel for 2 h and 50 min before being transferred to a PVDF membrane using a semi-dry transfer unit (BioRad, Hercules, CA, USA). All blots were initially stained with Ponceau S for protein visualization. Membranes were then blocked and incubated overnight at 4 °C with the appropriate primary antibodies. Both the nebulin N-terminal antibody and the SH3 antibody were provided by Dr Siegfried Labeit (Nebulin N-term 1:1000 rabbit, SH3 1:200 rabbit, University of Heidelberg, Mannheim, Germany). Secondary antibodies used were conjugated with infrared fluorophores for detection (1:20 000 goat anti-rabbit CF680, Biotium, Fremont, CA, USA and 1:20 000 goat anti-mouse CF790, Biotium). Infrared western blot was analyzed using an Odyssey CLx Imaging System (Li-Cor Biosciences, NE, USA). MHC was visualized by Ponceau S and quantified with One-D scan EX software (Scanalytics Inc., Rockville, MD, USA).

Thin filament length measurement

Small fiber bundles were isolated from thawed biopsies. The ends of the bundles were attached to aluminum T-clips and the solution replaced with fresh relaxing solution. Bundles were stretched ~50% of their base length. Relaxing solution was then replaced with 4% formaldehyde solution and muscles were fixed overnight. After fixation, muscles were washed with phosphate buffer saline (PBS) and embedded in Tissue-Tek O.C.T.compound (Ted Pella Inc) and stored at -80 °C. The O.C.T. embedded specimen was sectioned into 5 µm thick (Microm HM 550; Thermo Scientific) and placed on glass slides (Fisher Scientific, size: 25X75X1 mm). Fixed tissues were permeabilized with 0.2% Triton X-100 in PBS for 20 min at room temperature on a light box to bleach out the background fluorescence, blocked with 2% bovine serum albumin (BSA) and 1% normal donkey serum in PBS for 1 h at 4 °C, and incubated overnight at 4 °C with Alexa Fluor 488–conjugated phalloidin (1:1000; Invitrogen). The sections were then washed three times with PBS for 15 min and coverslips (Fisher Finest Premium Cover glass, size: 22X50X1 mm) were mounted to glass slides using Aqua Poly/Mount (Polysciences Inc.). Images were captured using a Deltavision RT system (Applied Precision) with an inverted microscope (IX70; Olympus), a × 100 objective, and a charge-coupled device camera (CoolSNAP HQ; Photometrics) using SoftWoRx 3.5.1 software (Applied Precision). The images were then deconvolved using SoftWoRx. Deconvolved images were reopened in ImageJ (http://rsb.info.nih.gov/ij), then the 1D plot profile was calculated along the myofibril direction. The plot profile was analyzed using Fityk0.9.8 (http://fityk.nieto.pl). A custom 'rectangle + 2 half Gaussian' function was used for analyzing phalloidin-stained images that consisted of a rectangle that was flanked by two half Gaussian curves. To account for actin overlapping in the Z-disk which creates a small bump in the center of the rectangle, we developed a special script designed for Fityk that de-activates the center points within the rectangle fit. This improved the subsequent fit for the 'rectangle + 2 half Gaussian' function. Thin filament length was calculated as half the width of the rectangle plus half the width of the Gaussian fit at half maximum height. SL was calculated from the distance between the centers of two adjacent Gaussian fits. We analyzed a large number of images and determined thin filament length within the SL range of 2.8–3.2 µm for all patients and controls. TFL measurement for patient 180 and one controls was performed at SL range of 3.5 -4 µm. The obtained thin filament length measurements were plotted against the fiber type 1 content of the biopsy. Linear regression did not reveal a significant effect ($p = 0.6$). To address the effect of previously frozen tissue on thin filament length, a study was conducted on mouse EDL muscle in which results on fresh muscle were compared with that of frozen/stored/thawed muscle. Thin filament length measurements at a wide range of sarcomere lengths revealed no difference between fresh and frozen tissues. Thus, using frozen tissue to study thin filament length is valid.

Statistical analyses

All data are represented as average ± SEM (standard error of the mean). GraphPad Prism 10.02 was used to calculate statistics. For statistical analysis one-way ANOVA, and the t-test with multiple testing corrections were used, as appropriate. To compare nebulin level, TFL or mechanical features between low and normal level nebulin patients, Student's t-test were used. To compare maximal or sub-maximal tensions between controls and each of patients, nested analysis was used. To get the relationship between nebulin level and transcript level, TFL or OM sensitivity, linear regression model was performed.

Results

Variant analysis using RNA sequencing

To assess the effects of *NEB* pathogenic variants on nebulin transcript level and mRNA processing, we performed RNAseq analysis on skeletal muscle biopsies of 10 NEM2 patients (Supplementary Table 1 presents clinical details) and as controls, three healthy individuals who did not exhibit any muscle-related conditions. Patient 144 had a homozygous deletion of exon 55, whereas the remaining patients

exhibited compound heterozygous variants, including splice site pathogenic variants, truncations, frameshifts, duplications, insertions, or deletions (variant details in Table 1). A summary of all RNA-seq findings (explained below in detail) can be found in Supplementary Table 2.

Several regions in *NEB* are known to undergo alternative splicing (the central SR region exons 63–66, 82–105, and 143/144; the Z-repeat region exons 166–177) and it has been proposed that variants in these regions may have a relatively mild pathogenic effect compared to variants elsewhere in the gene [19, 39, 105]. We performed alternative splicing analysis and studied RNA processing in each sample. Findings confirm alternative splicing in the Z-repeat exons 166–177, as well as the SR exons 143/144, 82–105 and 63–66, as shown by their PSI values below 100% (Fig. 1a). Moreover, we observed the exclusion of specific exons in several patients, which could be explained by the known pathogenic variants present in those individuals. For instance, patient 144, who had a homozygous deletion of exon 55, exhibited a PSI of 4% for that exon, confirming the near absence of this exon in the majority of nebulin mRNA molecules in this patient (Fig. 1a). Similarly, patient 2385, with a deletion of exon 77 on one of their *NEB* alleles, displayed a PSI of 46% for exon 77, which is close to the expected 50% PSI. Additionally, in patient 151, exon 30 was skipped in 85% of the nebulin transcripts. This patient carried a 4-base pair deletion in intron 30 (c.3042 + 3_3042 + 6del), classified as a variant of uncertain significance (VUS) in the ClinVar database. The splice site analysis further supported the pathogenic nature of this intronic variant.

Pathogenic truncation variants are frequently observed in NEM2 patients (Table 1). To better understand the impact of pathogenic truncation variants on the stability of *NEB* mRNA in these patients, we conducted an allelic imbalance analysis. This involved summing the reads based on their position and comparing the number of mutated alleles to wild-type alleles at the site of the truncation variants. A lower ratio of mutant to WT alleles would suggest that the mutated transcript undergoes nonsense-mediated decay (NMD) [5]. Our findings, shown in Fig. 1b, reveal allelic imbalance in patients 2296, 2486, 3424, 4526, and 180, all of whom harbor truncation pathogenic variants. This supports the notion that pathogenic truncation variants in these patients affect *NEB* mRNA stability and lead to NMD of the mutated transcript.

To evaluate the overall transcript level of nebulin, we normalized nebulin read counts to titin, to account for varying ratios of muscle fibers contained within each biopsy sample and for differences in library size. Results depicted in Fig. 1c show that nebulin transcript levels of patients are either relatively normal (patients 2385, 4001, 4526 and 144) or are reduced (patients 3424, 180, 2486 and 2622). Varying degrees of nebulin transcripts levels might be due to different NMD efficiency or skipping of exons carrying stop codon (Supplementary Table 2).

Additional analysis was also performed on patient 180. According to genetic testing, one of the *NEB* pathogenic variants in this patient is a four-copy gain in the triplicate region of nebulin. The triplicated (TRI) region of nebulin normally consists of 3 groups of exons (exons 82–89, 90–97, 98–105) each representing 2 SRs for a total of 6 SRs [32]. Four copy-gain results in ten TRI repeats, which if transcribed and translated fully would result in 8 more SRs in nebulin in this patient [32]. To investigate the TRI expression level, we normalized read counts of each exon in this patient by exon length and then measured the ratio of normalized read density of all exons relative to controls. Figure 1d illustrates the results. The normalized read density of exons within the triplicate region (82–105) varied somewhat but was around twice as high as controls in most exons. Some exons were closer to control read density (exons 87–88 and 102–105) while others were increased about three-fold (exons 94–97). Mapping of RNA-seq reads carries uncertainty due to the repetitive nature of the region. Overall, increased normalized read density versus controls would implicate an addition of 2859 bases versus controls, which would equate to an addition of 28 simple repeats (two TRI copies or four SRs) (Supplementary Table 3). Thus, in contrast to the genetic testing report of this patient which shows four more TRI repeats at DNA level, analysis at the transcription level shows only two additional TRI repeats. Furthermore, analysis of allelic imbalance of this patient's truncation pathogenic variant in exon 157 indicated that transcripts originating from the other allele accounted for only 17% of all transcripts (Fig. 1b). This suggests degradation of transcript of this allele by NMD.

Partial intronic inclusion and activation of cryptic splice site was consistently observed in all patients with variants at donor splice sites (Patients 2385, 4001, 2622, 151, and 3424), which resulted in atypical alternative splicing patterns, as detailed in Fig. 2a. Cryptic splice sites are normally inactive or utilized at low levels unless prompted by mutation near authentic splice sites [71]. While it is commonly believed that the activation of cryptic splice sites may play a role in a wide range of genetic diseases [31], the concept of reversing aberrant splicing through the targeted activation of cryptic splice sites has been suggested as a potential therapeutic strategy [79]. The activation of cryptic splice site in NEM2 patients led to either in-frame (4001, 2622 and 3424) or out-frame (2385 and 151) intronic inclusion. In-frame intron inclusion could lead to production of nebulin transcripts with increased repeat lengths. Moreover, the transcripts produced by cryptic splice sites showed different percentages in NEM2 patients (Fig. 2a and Supplementary Table 2). The percentage of transcript produced by cryptic splice site activation, in-frame or out-frame intronic

Table 1 Genetic information of patients with NEM2

Patient ID		Mutation details in *NEB* gene	Mutation consequence	Mutation type	Clinical significance	Mutation site on nebulin protein
2385	1	Exon 32 c.3252_3255 + 3delTGACGTA	Results 7 bp deletion	Deletion	Likely pathogenic	SR3 R6,R7
	2	2.7 kb deletion exon 77 g.152,469,299 in intron 77 g.152,471,995 in intron 76	Results 2697 deletion including exon 77	Deletion	–	SR14 R7 / SR15 R1,R2,R3
2296	1	Exon 112 c.17654G > A	Results generation of stop codon in exon 112	Truncation	Pathogenic	SR24 R2/R3
	2	Exon 175 c.24771delT	Results deletion in exon 175 leading to stop 19 bp into exon 176	Frameshift	Pathogenic/likely pathogenic	M234/M235
2486	1	Exon 61 c.8425 C > T	Results generation of stop codon in exon 61	Truncation	Pathogenic/likely pathogenic in LOVD	SR10 R7 / SR11 R1,R2,R3
	2	Exon 171 c.24317 T > A	Results generation of stop codon in exon 171	Truncation	Pathogenic/likely pathogenic in LOVD	M230/M231
3424	1	Exon 85 c.13059 + 5G > A	Results point mutation in intron 85	Intronic point mutation	Likely pathogenic	SR16 R7 / SR17 R1,R2,R3
	2	Exon 169 c.24218C > A	Results generation of stop codon in last codon of exon 169	Truncation	VUS/pathogenic in LOVD	M228/M229 (Z-disk)
4001	1	Exon 32 c.3255 + 1G > A	Results donor splice mutation in junction of exon–intron 32	Splicing	Pathogenic	SR3 R6/R7
	2	Exon 110 c.17501_17502delinsc	Results insertion in exon 110 leading to stop codon 19 bp into exon 111	Frameshift	Pathogenic in LOVD	SR23 R7/SR24 R1
2622	1	Exon 80 c.12018 + 1G > A	Results donor splice site mutation in junction of exon–intron 80	Splicing	Pathogenic/likely pathogenic	SR15 R6/R7
	2	Exon 172 c.24458_24461dupAGAT	Duplication of AGAT in exon 172 leads to stop codon at the end of exon	Frameshift	Pathogenic/likely pathogenic	M231/M232
4526	1	Exon 109 c.17262G > A	Generation of stop codon in the middle of exon 109	Truncation	Pathogenic	SR22 R6/R7
	2	Exon 171 c.24318_24319insAA	Results insertion at the start of exon 171 leading to stop codon in exon 172	Frameshift	Pathogenic	M229/M230 (Z-disk)
144.0	1 2	Homozygous exon 55 deletion	Results in-frame 2502 deletion including exon 55	Deletion	Pathogenic	SR9 R5,R6
180.0	1	Four copy gain within the NEB triplicate repeat region	3 + 7 TRI repeats instead of 3 + 3	Duplication	Pathogenic	[SR16 R3,R4,R5] – [SR21 R7 / SR22 R1,R2,R3
	2	Exon 157 c.22936C > T (p.Arg7646*)	Results generation of stop codon in exon 157	Truncation	Pathogenic	M216/M217

Table 1 (continued)

Patient ID	Mutation details in *NEB* gene	Mutation consequence	Mutation type	Clinical significance	Mutation site on nebulin protein
151.0	1 Exon 10 c.822 + 1G > A	Results donor splice site mutation at the junction of exon–intron 10	Splicing	Likely pathogenic	M5
	2 and Exon 30 c.3042 + 3_3042 + 6del	Results 4 bp deletion of intron 30	Intronic deletion	VUS	R5 of SR2

**NEB* mutations are reported based on the transcript NM_001271208.1

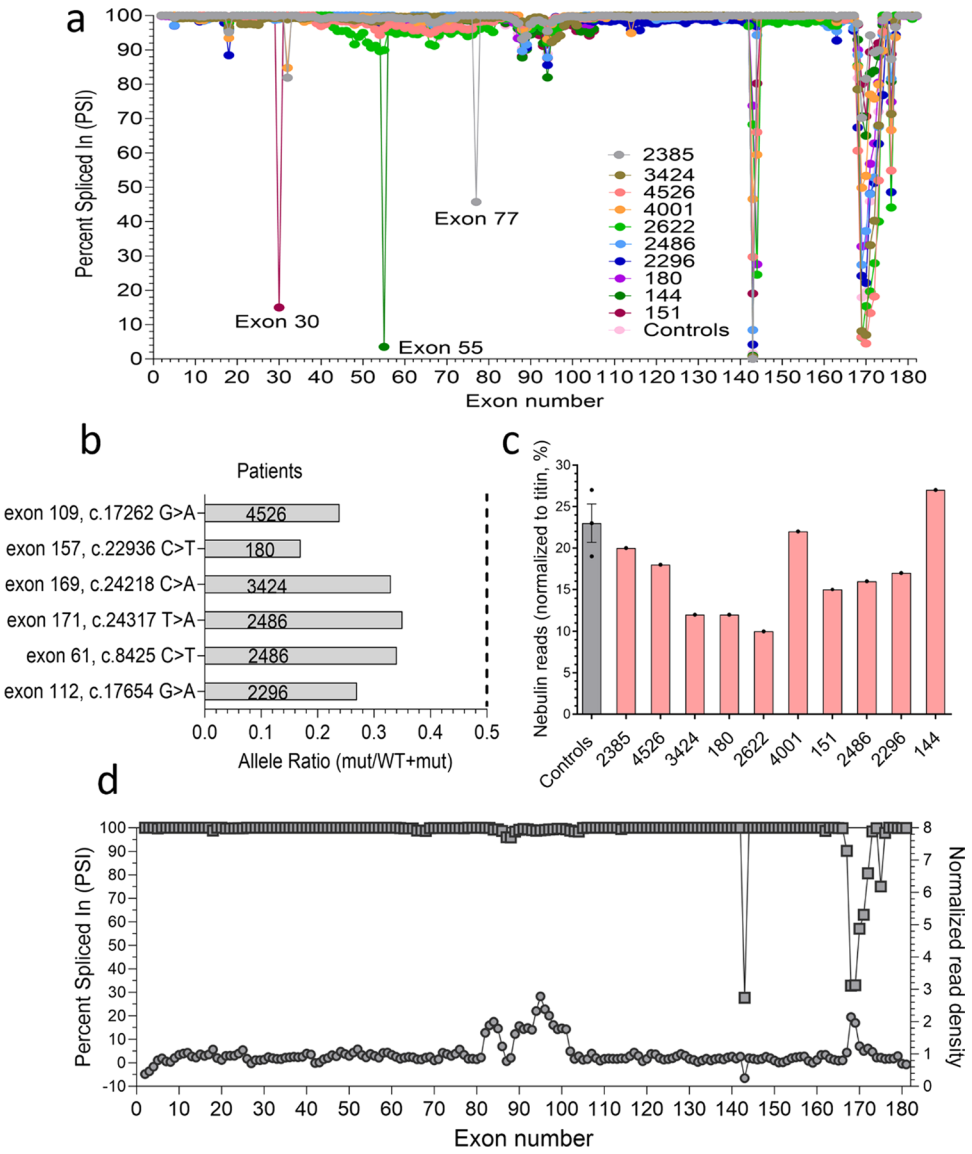

Fig. 1 Effect of pathogenic variants on *NEB* mRNA. **a** Alternative splicing pattern of *NEB* gene in NEM2 patients and controls. Percent spliced-in (PSI) values range from 0% (excluded in all transcripts) to 100% (included in all transcripts). **b** Allelic imbalance analysis for pathogenic truncation variants of NEM2 patients. The bars represent the expression ratio of the mutated allele to WT allele. The dotted line indicates the expected ratio if both alleles are expressed equally. **c** Read counts of NEB gene normalized by *TTN* reads. **d** Expression analysis of patient 180. The left Y-axis shows the PSI of *NEB* exons (square). To differentiate the copy gains in the triplicated region of *NEB*, the normalized read density of each exon is shown on the right *Y*-axis (circle), revealing a higher read density for exons in the triplicated region

inclusion and percentage of other transcript isoforms determine the different effects of cryptic splice site activation on the protein level. For instance, we detected partial inclusion of intron 32 in patients 2385 and 4001, which would result in an addition of 13 amino acids to repeat 7 of SR3. In patient 4001, this transcript version is in frame and constitutes around half of all nebulin isoforms, and it could have a significant impact on nebulin structure due to increasing repeat length. Interestingly, our results showed that intron inclusion in this patient would break up an actin binding

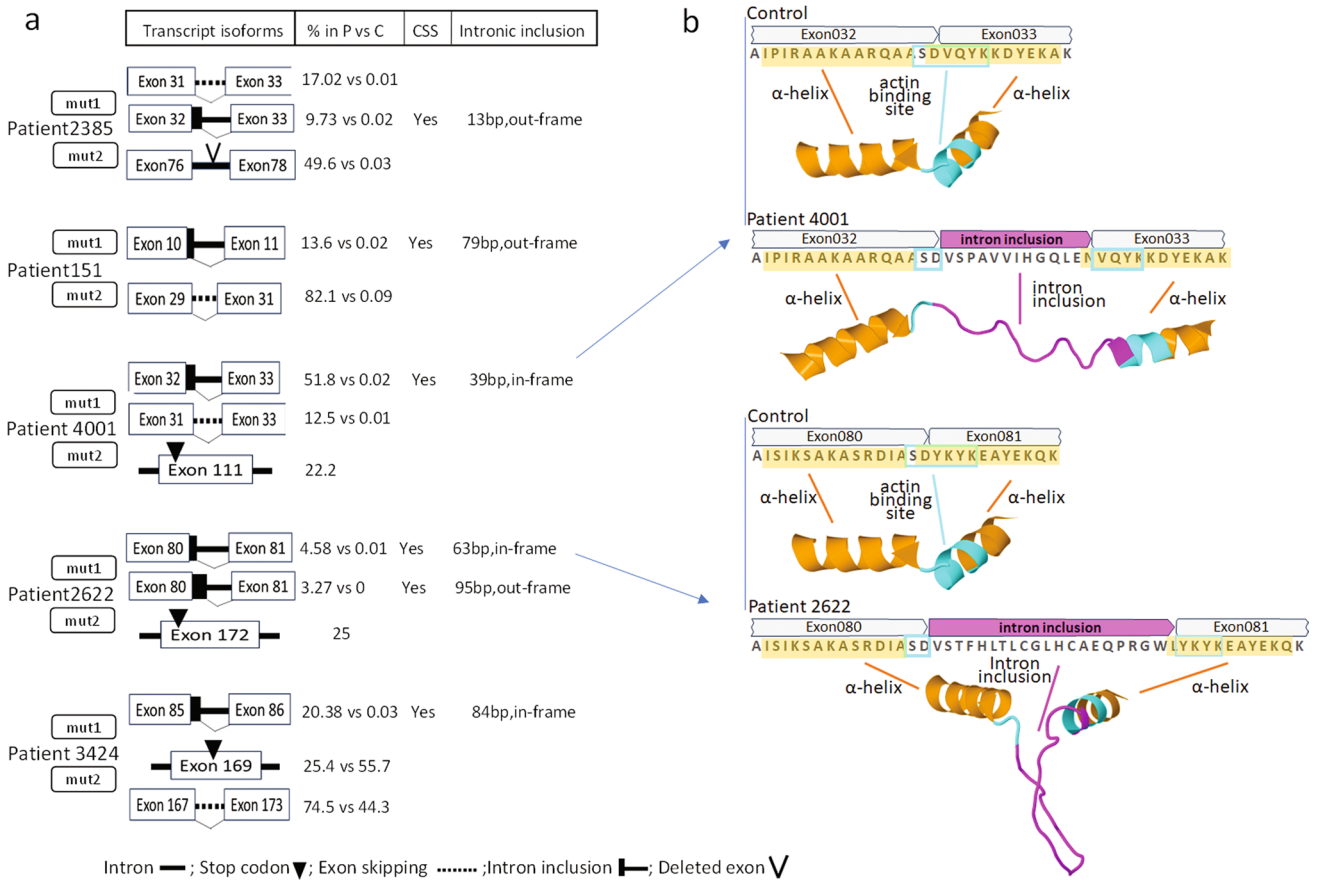

Fig. 2 Effect of *NEB* pathogenic splicing variants on transcript and protein. **a** In all patients with pathogenic splicing variants, cryptic splice sites are activated. For each patient and each pathogenic variant, transcript isoforms, percentage of transcript isoform in patient versus controls (% in P vs C), cryptic splice site activation (CSS) and intronic inclusion are indicated. The mutation (mut1 and mut2) details of each patient are in Table 1. The shown transcript isoforms are only those impacted by the pathogenic variant. **b** Sequence at the site of the splicing variant. In patient 4001 (top), pathogenic splicing results in 39 bp in-frame inclusion of intron 32 and consequently 13 amino acids are added (in super-repeat 3); in patient 2622 (bottom), 63 bp in-frame inclusion of intron 80 results in 21 additional amino acids (in super-repeat 15). The Alphafold predicted structure is shown with α-helix structure in orange, the intronic structure in pink and the actin-binding motif in cyan. In both patients, intronic inclusion leads to the addition of an unstructured region and disruption of the actin-binding site on nebulin

motif and add unstructured sequence into sections of nebulin which are predicted to be α-helical by ColabFold [53] (Fig. 2b and Supplementary Fig. 1a). This would lead to a mismatch between thin filament and nebulin-binding sites which need to be identically spaced. This finding provides insight into the underlying pathomechanism of pathogenic splicing variants in NEM2 patients.

Partial intron 32 inclusion in patient 2385 accounts for only 10% of transcripts because intron inclusion is out-of-frame due to the 7bp deletion (Fig. 2a and Supplementary Table 2) and leads to a stop codon and subsequent degradation by NMD. This might also explain why the ratio of the isoform with skipping of exon 32 relative to the isoform with intron inclusion is higher in patient 2385 (splice site deletion) than patient 4001 (splice site substitution). Other significant intron inclusion events occur in patient 2622, where inclusion of a portion of intron 80 adds 21 amino acids to repeat 7 of SR15. Like patient 4001, this intron inclusion event would add an unstructured sequence in the middle of nebulin's actin-binding motif (Fig. 2b and Supplementary Fig. 1b). In patients 3424 and 151, cryptic donor splice sites downstream of the pathogenic splicing variants were activated, but transcripts created from these sites would most likely be subject to NMD due to the presence of stop codons (Supplementary Fig. 2).

In summary, disease mechanisms that were revealed include degradation of nebulin transcript by NMD, exon skipping, and activation of cryptic splice sites that disrupt nebulin-binding sites to the thin filament. Additionally, the obtained results reveal for the first time that in some patients, longer than normal transcript can be produced.

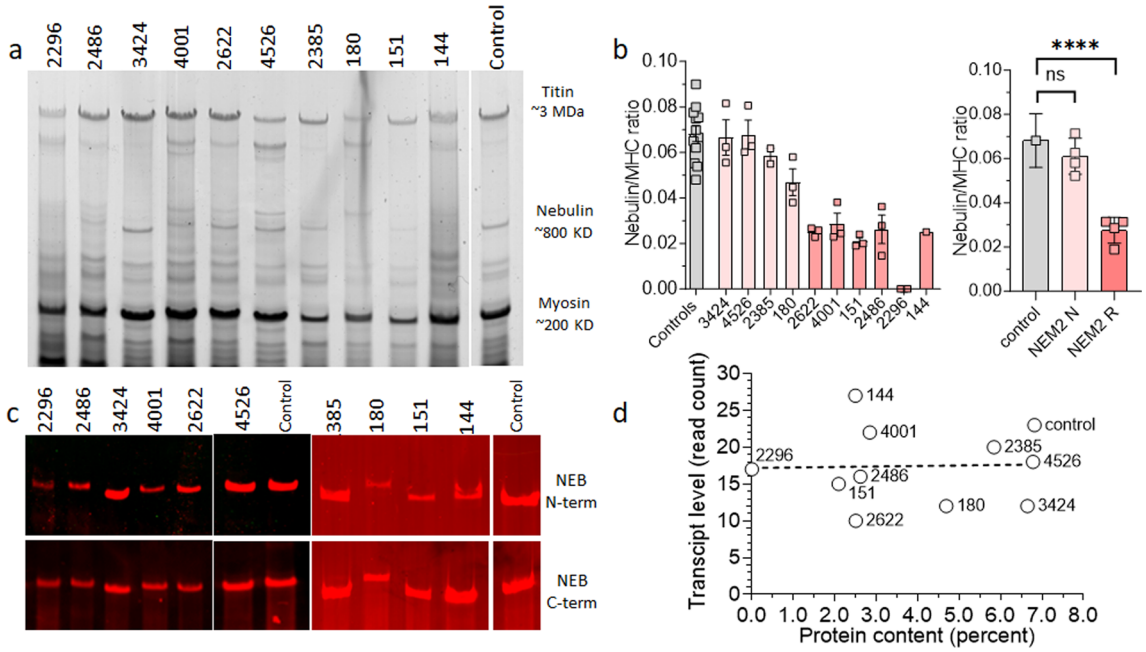

Fig. 3 Protein expression analysis. **a** Agarose gel electrophoresis reveals detectable nebulin in all patients, except for patient 2296. **b** (left) Nebulin quantification is expressed as nebulin/MHC ratio. Patients 3424, 2385, 4526, and 180 have nebulin levels similar to controls, while patients 2622, 4001, 151, 2486, 2296, and 144 have reduced nebulin levels. (right) Mean values per biopsy grouped as controls, NEM2 patient with normal nebulin (NEM2 N) and reduced nebulin (NEM2 R) expression and differences between groups analyzed with a nested one-way ANOVA. Asterisks indicate a significant difference between NEM2 R and controls. $*P < 0.05$, $**P < 0.01$, $***P < 0.001$, $****P < 0.0001$ and ns indicates no significant difference. **c** Western blot analysis using antibodies against the N-terminal and C-terminal ends of nebulin, targeting the M1-M3 and SH3 domains, respectively. Asterisk reveals slower migrating nebulin in patient 180. **d** Transcript level vs protein level in controls and patients shows lack of a correlation (slope of shown regression line not different from zero, $P = 0.9$). Note that in **b** (left) samples were analyzed independently 3 times (technical replicates) and that results from 3 controls were pooled

Nebulin protein expression

To assess the impact of *NEB* pathogenic variants on nebulin protein levels, we used sodium dodecyl sulfate-agarose gel electrophoresis (Fig. 3a, b) and western blot (Fig. 3c) techniques on lysates from muscle biopsies from both NEM2-patients and controls. Nebulin protein levels were normalized using myosin heavy chain (MHC) as a reference for protein loading. Previous studies have consistently reported a nebulin:MHC ratio of ~ 0.05–0.07across various skeletal muscle types and vertebrate species [13, 20, 35]. In line with this, our study revealed a nebulin:MHC ratio in control samples of 0.068 (Fig. 3b). When analyzing patients' samples, results segregated into two groups. Patients 3424, 4526, 180, and 2385 displayed nebulin:MHC ratios of 0.07, 0.07, 0.05, and 0.06, respectively. These ratios are all within the range of nebulin:MHC ratios observed in the control group (Fig. 3b-left). However, patients 4001, 2622, 2486, 144, and 151 displayed lower ratios, hovering around 0.03, except for patient 2296, where nebulin was undetectable on protein gels (Fig. 3b-left). When results were grouped accordingly, a significant reduction in nebulin expression was found in the patients with low expression (Fig. 3b-right). Furthermore, to determine if the patients expressed full-length nebulin, we utilized Western blotting with antibodies targeting the N-terminal and C-terminal ends of nebulin. The results revealed the presence of full-length nebulin in all patients (Fig. 3c). It should be noted that this full-length nebulin could potentially be mutated (such as those with in-frame deletions) or non-mutated. Finally, a limited electron microscopy study revealed that NEM2 patients with normal nebulin levels, displayed nemaline rods and Z-disk streaming, similar to seen in NEM2 patients with reduced nebulin (Supplementary Fig. 8).

The mobility of nebulin on agarose gel was similar for most patients, except for patient 180, who displayed visibly reduced nebulin mobility (see asterisk in Fig. 3c), suggesting a larger size of nebulin. This observation is consistent with this patient's pathogenic variants and aligns with the RNA-seq results, which showed higher read density of exons in the triplicated region. As discussed above, according to genetic testing, one of the *NEB* pathogenic variants in patient 180 involves a four-copy gain in the triplicate region of nebulin. However, RNA-seq

analysis showed transcripts produced by this allele contain 2858 additional base pairs (Supplementary Table 3) which accounts for two TRI copies and, thus, 4 more SRs. At the protein level, this is expected to result in a nebulin that is 108 kDa (4 × 27 KD) larger than normal, consistent with the reduced mobility of the nebulin band on the agarose gel for this patient. Additionally, as described earlier, the other allele of patient 180 carries a pathogenic truncation variant in exon 157, and accounts for only 17% of all transcripts, indicating its likely degradation through the NMD mechanism (Fig. 1b). It is noteworthy that protein gels do not reveal a band that is associated with this allele (Fig. 3a, c) implying another mechanism to prevent translation of transcript that carries the truncation mutation.

The transcript and protein data for each patient make it possible to evaluate if transcript and protein levels are correlated. Figure 3d reveals that the nebulin transcript' read counts for patients with low nebulin protein levels are not different from those with normal protein and the linear regression line has a slope that is not different from 0 ($P = 0.9$), i.e., there is no correlation between nebulin transcript and protein levels.

Effect of *NEB* pathogenic variants on TFL

Considering that nebulin plays a role in TFL specification [35], we investigated the effect of *NEB* pathogenic variant on TFL. To analyze muscle biopsies, we cut longitudinal sections and stained them with fluorescently labeled phalloidin to mark the actin filaments. TFL was measured according to the detailed procedures outlined in the Methods section. The results of all patients, except patient 180 (for reasons, see below) are presented in Fig. 4a. The TFL measurement revealed that patients with normal levels of nebulin (3424, 4526, and 2385) displayed mean thin filament lengths like those of the control group. In contrast, patients with reduced levels of nebulin (2622, 2296, 151 and 2486) exhibited a significant decrease in TFL compared to the controls (Fig. 4b). Linear regression analysis between TFL and nebulin content reduction revealed a significant negative relation ($P = 0.003$) (Fig. 4c). These findings support an important role of nebulin in determining TFL, as demonstrated by shorter TFL when nebulin protein levels are reduced.

RNA-seq experiments suggested a larger nebulin in patient 180. This was confirmed by agarose gel electrophoresis that showed a nebulin band with less mobility indicating that a larger nebulin protein is expressed (Fig. 4d-left). Therefore, a separate study was performed where bundles from patient 180 and one control biopsy was stretched to long sarcomere lengths (3.5–4.0 µm). TFL measurement showed that patient 180 had significantly longer thin filaments than controls (Fig. 4d-right).

Effect of *NEB* pathogenic variants on tension

It is well established that nebulin is important for normal contraction [103], therefore, we also investigated Ca^{2+}-activated force in single fibers. Frozen biopsies were thawed and membrane-permeabilized, and single fibers were carefully dissected and mounted in an apparatus for subsequent force measurements. These initial measurements were conducted at two activation levels: maximal (pCa(-log[Ca^{2+}]) 4.0) and submaximal calcium activation (pCa 6.75). After the mechanical study, fibers were fiber-typed (see Methods for details).

Several of the patients' biopsies expressed mainly slow fibers (type 1). Since we decided to study the effect of the slow myosin activator OM [50] (see below), the results of tension production are focused on type 1 fibers. The control group's type 1 fibers exhibited robust levels of maximal tension, averaging around 160 mN/mm^2. In contrast, the results from NEM2 patients displayed considerable variation. Several patients with relatively normal levels of nebulin (3424, 4526, 2385) showed the highest tensions, reaching approximately two-thirds of the control values. Conversely, patients with reduced nebulin levels experienced the lowest tensions, reaching only around one-third of the control values (Fig. 5a-left). Plotting the obtained tension values against nebulin protein reduction (Fig. 5a-right) revealed a significant negative relationship ($P = 0.004$). Similarly, submaximal activation resulted in reduced tensions among patients (Fig. 5b-left), and a negative relation ($P = 0.0004$) was identified between submaximal tension and nebulin protein reduction (Fig. 5b-right). Thus, the extent to which *NEB* pathogenic variants depress tension appears to be strongly dependent on the reduction in nebulin protein content.

Enhancing force development with OM

To assess the potential of OM in enhancing muscle force among patients with NEM2, patient fibers were activated in solutions with varying levels of calcium (pCa 8 to pCa 4) while being exposed to either 0.5 µM OM or vehicle. By analyzing the relationship between force and calcium concentration, we determined several parameters, including maximal tension (at pCa 4.0), submaximal tension (at pCa 6.75), pCa50 value (which represents the calcium concentration at half-maximal tension), and the Hill coefficient (nH), a measure of the cooperativity of activation.

Experiments revealed that OM did not affect type 2 fibers (Supplemental Fig. 3). This finding aligns with previous research indicating that OM selectively affects fiber types expressing the *MYH7* gene, such as cardiac muscle and type 1 skeletal muscle fibers [26, 48, 56]. No significant effect on maximal tension was observed when comparing OM-treated type 1 fibers with those treated with vehicle, in either

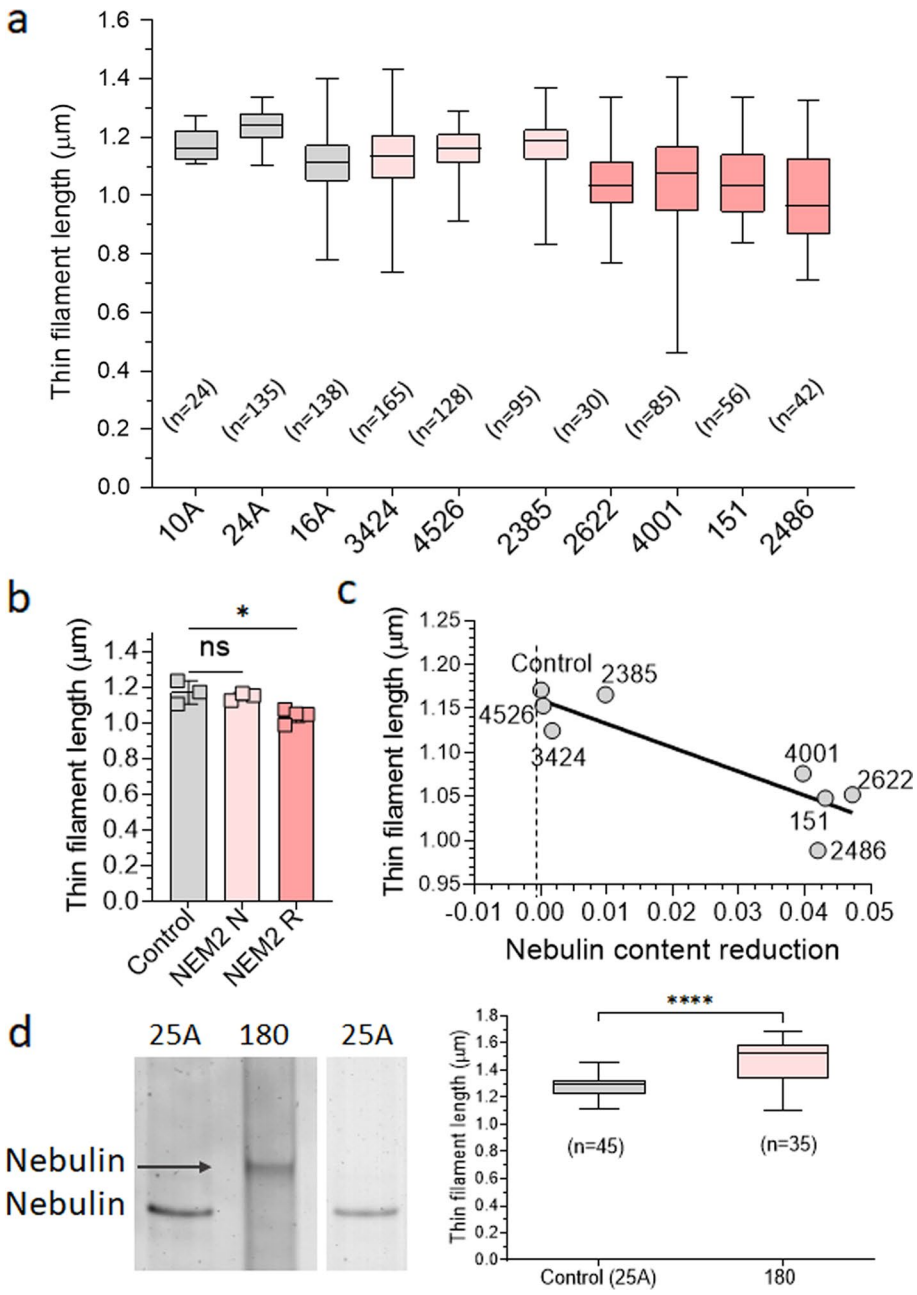

Fig. 4 Thin filament length (TFL) in muscle fibers from NEM2 patients and controls. **a** TFL was measured based on phalloidin staining of actin filaments of NEM2 patients (except patient 180) and controls. Measurements were obtained in the 2.8–3.2 mm sarcomere length range. **b** Mean TFL per biopsy, grouped with NEM2 biopsies segregated according to their nebulin expression level (N for normal and R for reduced, see Fig. 3 for details). One-way ANOVA analysis reveals significantly reduced TFL in NEM2-R samples. **c** Mean TFL vs. nebulin content reduction (nebulin:MHC ratio in controls minus in patients). The slope of the linear regression line is significantly different from zero ($P = 0.003$). **d** (Left) electrophoretic analysis of control and patient 180 samples on a 1% agarose gel reveals reduced mobility of nebulin in patient 180. (Right) TFL measurements (sarcomere length range 3.5–4.0 mm) show longer TFL in patient 180 (1.469 mm) than control (1.275 mm). Data are presented as box and whisker plots. Asterisks indicate a significant difference between NEM2 R and controls. $^{*}P < 0.05$, $^{**}P < 0.01$, $^{***}P < 0.001$, $^{****}P < 0.0001$ and ns indicates no significant difference

patients or controls (Supplemental Fig. 4). This suggests that 0.5 µM OM treatment does not reduce the force deficit observed at maximal activation levels in these patients, which is consistent with earlier studies [48, 56].

In type 1 fibers, the force-pCa plots exhibited a notable leftward shift in fibers treated with 0.5 µM OM compared to the control group (vehicle) (Fig. 6a). This shift was characterized by an increased pCa50 value (Fig. 6b) and a decrease in nH (not shown). Moreover, comparing the shift in pCa50 between control subjects and NEM2 patients, we observed a more pronounced effect in the NEM2 group (Fig. 6c). These findings indicate that OM enhances calcium sensitivity, with a greater impact observed in NEM2 biopsies. Additionally, submaximal tension measurements demonstrated significant OM-based increases (87–318%) in both control and NEM2 biopsies (Fig. 6d, e). Notably, the tension increase was more prominent in NEM2 patients and showed an inverse relationship with nebulin protein content (Fig. 6f) i.e., the increase in tension is highest in patients with the lowest level of nebulin.

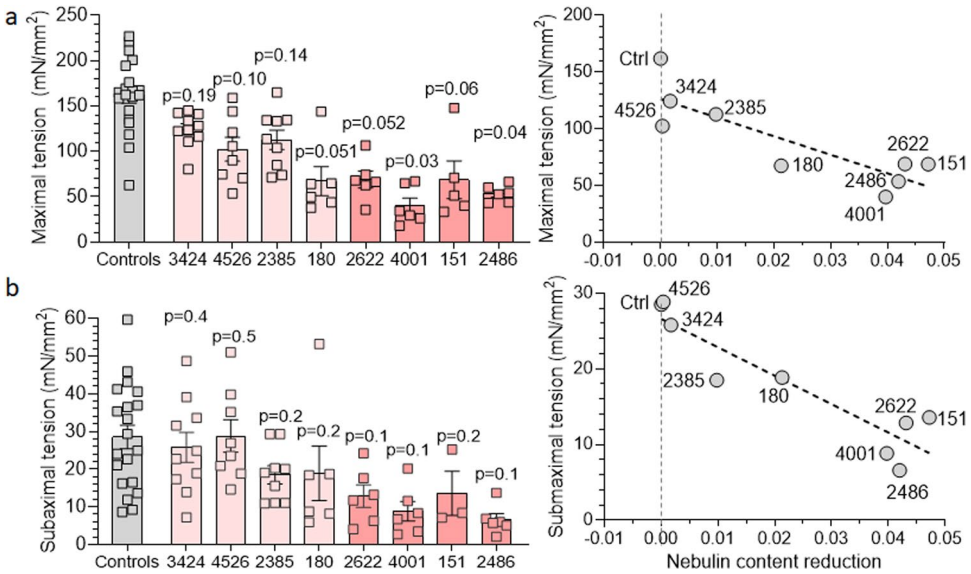

Fig. 5 Tension production in control and NEM2 patients. **a** Maximal tension at pCa 4.0 and **b** submaximal tension at pCa 6.75 of type 1 fibers in control and NEM2 fibers. Left: results from individual fibers; right: mean tension vs nebulin protein content. Both maximal and submaximal tensions negatively correlate with nebulin content reduction (NEB/MHC ratio in controls minus in patients). Note that each data point in **a**-left and **b**-left reflects one fiber, and in **a** and **b** right the mean of all fibers per biopsy. Data were analyzed by linear regression analysis and obtained *P*-value for slopes are 0.004 (**a**) and 0.0004 (**b**). *P* values on each bar in **a** and **b** left are obtained by nested t-test analysis to compare tension between each patient and controls

Effect of OM on rate of tension development (*ktr*) and dynamic stiffness

Utilizing membrane-permeabilized single muscle fibers we studied the effect of OM on *Ktr at* maximal (pCa 4) and submaximal (pCa 6.75) activation levels. A series of step length changes was also imposed and the ensuing force transients were fitted to a non-linear distortion recruitment model, to extract the number of attached cross-bridges (ED) and their attachment and detachment rates [52]. To keep the workload manageable, we used fibers from controls and two patients: patient 2385 with normal nebulin and patient 2486 with reduced nebulin. Experimental details and typical force recording are provided in the Methods section and Supplementary Fig. 5.

Findings show OM leads to a reduction in *ktr* for controls and both patients at both pCa 4 and pCa 6.75 (Fig. 7a). This decrease can be attributed to the extended duration of the strongly bound state of myosin heads in the presence of OM, culminating in slower cross-bridges cycling [104]. Moreover, at pCa 4, OM treatment does not alter ED [6, 9, 23, 68] (Fig. 7b-left) but at pCa 6.75 OM increases ED in controls and patients (Fig. 7b-right).

Finally, we measured detachment (c) and attachment (b) rate of cross-bridges at pCa 4. (Due to the low force levels at pCa 6.75, only a limited data set could be obtained, see Supplementary Fig. 6). As shown in Fig. 7c, OM-treated fibers exhibited significantly decreased c in controls and both patients. However, OM treatment resulted in reduced b in only controls and patient 2385 and in patient 2486 did not show an effect (Fig. 7d).

Discussion

We investigated a cohort of NEM2 patients, each with distinct pathogenic variants, and studied their impact on mRNA, protein, and functional levels. We found that pathogenic truncation variants reduce *NEB* mRNA stability and lead to NMD of the mutated transcript. Additionally, a high occurrence of cryptic splice site activation and intronic inclusions was detected. In several NEM2 patients, intron inclusions added an unstructured region to nebulin's simple-repeats, which is expected to disrupt the actin-binding sites of nebulin. At the protein level, the expression level of nebulin varied in NEM2 patients, between close to normal and very low, and no correlation between nebulin transcript and protein levels were found. Force and TFL were reduced in NEM2 patients (with the exception of one patient exhibiting longer thin filaments), and the effect was most severe in patients with the lowest nebulin levels. Finally, OM increased submaximal force levels and the effect was highest in patients with the lowest nebulin level. Below, we elaborate on these results.

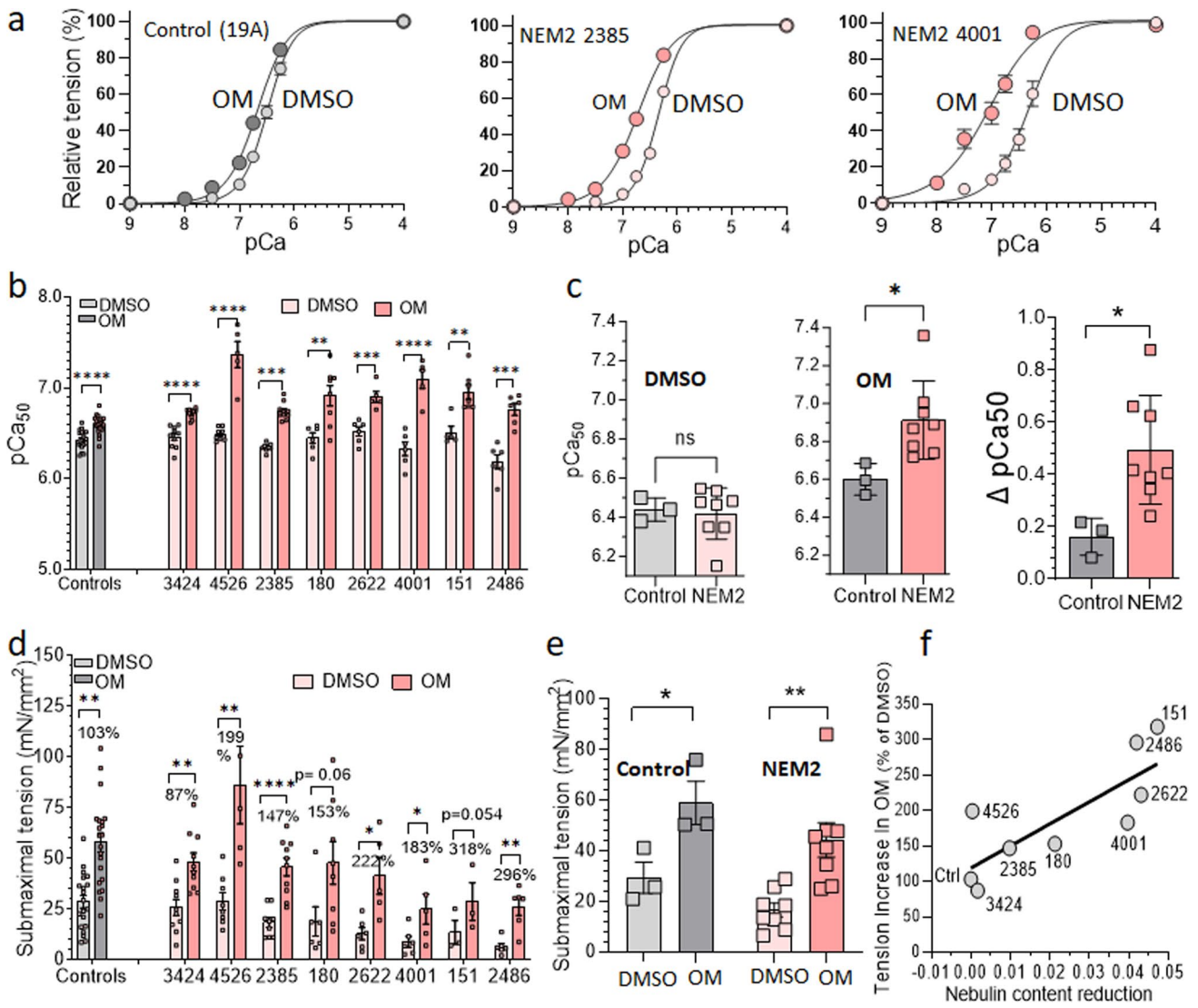

Fig. 6 Effect of omecamtiv mecarbil (OM) on calcium-sensitivity and submaximal force. **a** Example force-pCa curves in control and NEM2 patient with normal nebulin level (2385) or reduced nebulin (4001). OM left shifts the curves. **b** Summarized pCa50 data of all biopsies revealing that OM increases pCa50 in all cases (each data point represents a separate single fiber). **c** pCa50 of the control and NEM2 biopsies grouped and analyzed in an unpaired t-test showing no difference between groups in DMSO (left) but a significantly higher pCa50 in OM in NEM2 patients (middle) and consequently a larger DpCa50 in NEM2 patients (right). **d** Submaximal tension (pCa 6.75) of control and NEM2 fibers is increased by OM in all patients and controls. **e** *t*-test analysis shows that summarized tension of control and NEM2 fibers are significantly increased by OM. **f** Tension increase in OM scales with nebulin content reduction (NEB/MHC ratio in controls minus in patients) (*P* value of regression line: 0.01). Asterisks indicate a significant difference between DMSO and OM-treated fibers and ns indicates no significant difference. $*P < 0.05$, $**P < 0.01$, $***P < 0.001$, $****P < 0.0001$

Variant analysis and effect on nebulin expression

Based on quantification of nebulin protein levels, patients were divided into two groups: one with approximately normal levels of nebulin protein (average nebulin/MHC ratio of 0.06) and one with reduced levels (average nebulin/MHC ratio of 0.03). The overall *NEB* transcript level was not correlated with nebulin protein levels (Fig. 1c). This discrepancy is consistent with other genome-wide studies that also have shown that the correlation between levels of mRNA and protein is generally poor, hovering around 40% explanatory power across many studies [12, 90]. This may be due to several factors, such as variations in translational rates or protein turnover, as well as the presence of post-transcriptional/translational mechanisms that regulate nebulin expression.

Previous studies have proposed that partial SR deletion is not tolerated in nebulin [25, 35, 61] because it causes a structural mismatch between nebulin actin binding sites and the thin filament, and this prevents nebulin

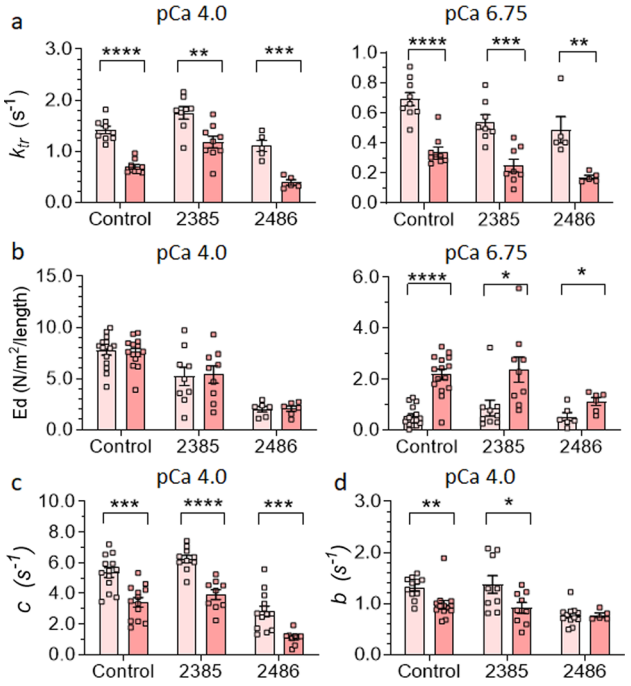

Fig. 7 Effect of Omecamtiv mecarbil (OM) on rate of force redevelopment (*ktr*) and dynamic stiffness and crossbridge kinetics. **a** OM results in lower *ktr* in controls and patients 2385 (normal nebulin) and 2486 (reduced nebulin) at both pCa4 (left) and pCa6.75 (right). **b** OM treatment does not affect dynamic stiffness (Ed) at pCa4 (left) but increases it significantly at pCa6.75 in controls and both patients (right). **c** OM treatment lowers the detachment rate of cross-bridges (*c*) at pCa4 in controls and both patients. **d** OM treatment lowers the attachment rate of cross-bridges (*b*) at pCa4 in controls and patient 2385. Asterisks indicate a significant difference between DMSO and OM-treated fibers and ns indicates no significant difference. $*P < 0.05$, $**P < 0.01$, $***P < 0.001$, $****P < 0.0001$

incorporation in the thin filament and enhances nebulin's vulnerability to proteolysis [1, 61]. Hence, normal transcript but reduced protein levels in some of NEM2 patients might be due to such structural mismatch between nebulin and the thin filament. This can explain the reduced nebulin levels in patients with full exon deletion which leads to partial SR deletion. For instance, patient 144, who is homozygous for the deletion of exon 55, has normal transcript levels but reduced protein levels which is likely caused by partial deletion of SR9. Similarly, nebulin levels might be reduced in patient 151 (82% skipping of exon 30) due to partial deletion of SR2. Disruption of binding sites on nebulin can also be caused by activation of cryptic splice sites and subsequent intronic inclusions. For instance, in patient 4001, the *NEB* transcript appears normal, yet the protein level is diminished. Prediction of nebulin structure in this patient revealed a partial intronic inclusion at the site of the pathogenic splicing variant and this results in an unstructured region which disrupts the actin binding sites on nebulin (Fig. 2b).

Splicing analysis of patient 2385 revealed that transcripts in this patient have either exon 77 skipped, or exon 32 skipped, or they have cryptic splice site usage that results in an out-of-frame transcript due to a 7 bp deletion (Fig. 2a and Supplementary Table 2). It is to be expected, therefore, that due to the above discussed nebulin-thin filament structural mismatch, nebulin protein is degraded, yet protein levels are normal in this patient (Fig. 3b). We speculate that considering that skipping exon 32, which encodes SR3 which is close to the nebulin's end, may not be as harmful as skipping exons located more centrally. Another potential scenario could be that post-translational modifications may contribute to the incorporation of mutated nebulin into thin filaments, rendering it resistant to protein degradation. Further investigation is required to explain the normal nebulin level in this patient.

Pathogenic variants affecting donor splice sites were identified in five NEM2 patients (3424, 2622, 4001, 151 and 2385). The transcripts originating from these alleles exhibited partial intron inclusion and the activation of cryptic splice sites (Fig. 2a and Supplementary Table 2). Given that splice site mutations are the most prevalent type of pathogenic variants within the *NEB* gene [42], it is important to consider the potential impact of these frequently occurring cryptic splice sites when interpreting identified *NEB* gene variations. In our cohort, two intronic variants were initially classified as VUS. However, our results demonstrate that both variants have pathogenic implications, either by inducing exon skipping (patient 151) or by activating cryptic splice sites and intron inclusion (patient 3424). These findings underscore the need to optimize cryptic splice-site prediction algorithms or perform transcriptomic studies for a more accurate interpretation of the functional implications of splice site and intronic mutations within the *NEB* gene.

Our findings revealed allelic imbalances for all pathogenic truncation variants in our patient's cohort (Fig. 1b), showing their deleterious impact on *NEB* mRNA stability and their role in triggering NMD. This conclusion was further substantiated through protein analysis, as we were unable to detect any truncated nebulin protein by western blot (Fig. 3c). Absence of truncated proteins is consistent with the notion that transcripts containing premature stop codons (PTC) undergo degradation via the NMD pathway and support the role of NMD in regulating *NEB* transcripts. It is known that not all PTCs trigger NMD [46] and that the position of PTC [41, 55], gene, length of exons carrying PTC mutations [29, 45] and tissue type [43, 106], all determine the efficiency of NMD. As an example, several studies have shown that *TTN* truncating variants (TTNtv) are not subject to substantial NMD [22, 70, 75] which implies inefficiency of NMD to degrade TTNtv transcripts [34] and as a result truncated proteins can be produced [7, 22, 28, 70, 89]. Furthermore, the allelic ratio for pathogenic truncation variants in our study is not zero (0.15–0.35) which suggests

that the absence of truncated nebulin is also likely to include more effective protein degradation of truncated nebulin compared to truncated titin.

Effect of *NEB* pathogenic variants on TFL and tension production

Nebulin's role in TFL regulation and force generation is well studied in mouse models [3, 61–64, 102]. Here we addressed how nebulin pathogenic variants influence TFL and force in NEM2 patients. Results underscore the pivotal role of nebulin in governing TFL, as evidenced by a notable negative relation between loss of nebulin and TFL (Fig. 4c). Patients with reduced nebulin levels exhibited significantly shorter TFL in comparison to controls. Conversely, patients with normal nebulin demonstrated TFL similar to controls (Fig. 4b). Furthermore, patient 180, with a larger nebulin size, exhibited a longer TFL relative to controls (Fig. 4d). RNA-seq results showed transcripts of this patient with 2859 additional bp comparing to controls which equates to two more TRI copies (Supplementary Table 3), or four additional SRs. TFL can be expected therefore to be longer than in controls, and this is what was measured (Fig. 4d-right). Longer TFL in this NEM2 patient reveals, for the first time, that not only shortened but lengthened TFL is implicated in the pathomechanism of NEM2. This finding aligns with previous study which suggested that *NEB* can tolerate deviations of one TRI copy, whereas the addition of multiple copies may be pathogenic [32]. Our studies also showed that the transcript level of this patient is reduced (Fig. 1c), but nebulin protein level is relatively normal (Fig. 3b). It is possible that the two-copy gain may disrupt the stability or secondary structure of the mRNA [32], which is reflected in the lower level of *NEB* transcript, but does not impact protein level, possibly due to tighter binding between longer nebulin and thin filament which increases protein stability.

Our study underscores that nebulin is critically important for TFL regulation in skeletal muscles. However there are other proteins that play a role in TFL regulation as well, such as the pointed-end associated leiomodin 2 (LMOD2)[35] and leiomodin 3 (LMOD3). Mutations that result in LMOD3 deficiency result in NEM with a reduced TFL [106]. NEM patients with ACTA1 mutations have also been reported to have shorter thin filament lengths whereas TFL has been reported unchanged in TPM or TNNT-based NEM [101].

We observed a negative relation between reduction of nebulin level and tension production, both for maximal and submaximal tensions (Fig. 5). This correlation underscores that patients with relatively normal nebulin exhibit a less pronounced reduction in tension compared to those with reduced nebulin. The diminished tension observed in patients with nebulin deficiency can be attributed to factors such as altered cross-bridge cycling kinetics, changes in thin filament and sarcomere structure and myofibrillar misalignment [3, 8, 40, 59, 61, 62]. Our finding that force is reduced in some patients despite a relatively normal level of nebulin bears resemblance to the findings in a mouse model of typical nemaline myopathy [49] wherein a decrease in specific force was noted despite the presence of normal nebulin levels. The force deficit observed in this mouse model was attributed to changes in thin filament structure and less organized myofibrils [49] and a similar explanation might hold here.

It is also relevant to note that TFL was determined in the present study by using optical techniques, and this provides an average length but cannot determine the variation in thin filament length. In previous immunoelectron microscopy studies on mouse muscle it was shown that when nebulin levels are reduced, thin filaments are shorter *and* vary greatly in length. The shorter length and length variation lowers the force on the descending limb of the force-sarcomere length relation as well as lowers the maximal force at optimal sarcomere length (see Fig. 3 in [8]). Thus, it is likely that both the reduction and variation in TFL explains the effects on tension that we measured, with the most severe effects in patients with the lowest level of nebulin because the TFL is most severely affected. Patient 180 is unique because it has thin filaments that are *longer* than normal. The consequence of longer TFL is that the force-sarcomere length relation is right shifted [27] and that the operating sarcomere length might include the ascending limb where force is less than optimal.

In summary, the studies on NEM2 patients support the critical importance of a normal level of full-length nebulin for thin-filament length regulation and force production. Both a reduction and an increase in TFL are deleterious, and the uniformity in TFL is critical as well.

Effect of OM on force production

OM is a small-molecule activator that was developed for the treatment of heart failure which increases the calcium sensitivity of force production by binding to cardiac myosin (*MYH7*) [26, 67, 82]. OM is also effective on type 1 skeletal muscles [48], because these fibers express the same myosin isoform as found in cardiac myocytes [77]. Given the large number of type 1 fibers in humans [76, 86], and the additional shift in NEM patients toward type 1 fibers [40, 63, 78] OM is an attractive candidate to counteract muscle weakness in NEM2 patients.

OM treatment increases calcium sensitivity (Fig. 6a, b) and consequently submaximal force production (Fig. 6d) of slow fibers in all NEM2 patients. This finding is consistent with the mechanism proposed for OM which suggests OM binds to myosin, leading to long-lasting, inactive myosin heads that cooperatively activate the thin filaments and

trigger binding of additional myosin heads that increase submaximal force [104]. The dynamic stiffness measurements in OM treated fibers were aligned with this mechanism revealing significantly higher ED of OM-treated slow fibers of both patients at pCa 6.75 relative to vehicle and no change of ED at pCa 4, indicating that at submaximal level of activation and in presence of OM, there are more strongly bound cross bridges. Moreover, it has been shown that OM disrupts the typical pathway of actin-myosin interaction, causing the detachment of myosin heads independent of ATP hydrolysis [104]. Thus, it can be postulated that OM treatment leads to reduction of tension cost due to long-lasting cross-bridges and ATP-independent detachment of cross-bridges. Our results of dynamic stiffness measurement agree with this notion as they show in OM-treated fibers slower *c*, supporting the effect of OM in reducing tension costs (Fig. 7c and Supplementary Fig. 6a).

Interestingly, OM enhanced submaximal force generation to a higher degree in NEM2 patients than in control fibers (Fig. 6f). This finding aligns with the study of Lindqvist et al. [48] in which OM had a greater effect in slow fibers from Neb cKO mice than from control fibers. The correlation between tension enhancement following OM treatment and the nebulin deficit may be explained by the different effects of nebulin pathogenic variants on *c*. Our results show that OM lowers *c* in the studied patient with reduced nebulin to a greater extent compared to controls or patient with normal nebulin (Supplementary Fig. 7). A lower *c* value indicates longer lasting myosin cross-bridges in the strongly bound state and thereby more force production. Whatever the underlying mechanism, the effect should be beneficial in patients with the lowest nebulin level who have the most severe force reduction and having a drug that has a great effect in these types of patients is highly needed.

For OM to be a beneficial therapy in NEM2 patients, it is important to avoid adverse effects. For instance, our findings demonstrate that 0.5 µM OM treatment reduces k_{tr} and *c* (Fig. 7a, c). Such reduction in cross-bridge cycling kinetics will adversely affect relaxation, which can be harmful in the heart. However, clinical trials have shown that OM is well tolerated without adverse effects up to ~ 1 µM of plasma concentrations in heart failure patients [30]. Thus, it is possible that the effects established in the present study using 0.5 µM OM will be able to increase skeletal muscle force in NEM2 patients without adverse cardiac effects.

Whether OM is effective in other NEM types has not been experimentally addressed. However, considering that OM enhances force generation by increasing calcium sensitivity, and in type 1 fibers only, its effectiveness is unlikely to extend to all NEM types. For example, some TPM2/3-based NEM patients with increased calcium sensitivity of force production have been identified [16, 18, 88] and further increasing calcium sensitivity with OM might not be desirable. Moreover, in NEM patients with mutations in KBTBD13, relaxation of muscles is slowed down [15]. Since OM is expected to further slow relaxation, because of longer lasting actomyosin bonds and the increased calcium sensitivity, OM might also not be suitable for these types of NEM patients. Another consideration is the fiber type switch seen in some NEM types towards fast fiber types [88] which will render OM ineffective. Thus, the OM effect is expected to scale with the fiber type 1 abundance and to be of potential use mainly in NEM types with a relatively high abundance of type 1 fibers.

Study limitations. The biopsies that were studied were not all from the same muscle type and the ages of patients and controls varied. However, most biopsies were from thigh muscles (vastus lateralis, quadriceps) and, additionally, in the mechanics studies, results were grouped according to fiber type. Results will, therefore, not be affected by differences in fiber type composition between muscle types. Three of the studied biopsies were from paraspinal muscles and when their results were omitted from our data set, conclusions and their statistical significances were not affected. We also assessed whether a correlation between age and nebulin protein or transcript level existed but found no significant correlation between age and nebulin levels (neither transcript nor protein). Finally, the main conclusions of our studies are derived from comparing NEM2 patients with either normal or reduced nebulin levels, i.e., these conclusions do not rely on controls (that were older than the patients). Thus, the conclusions of our work are not limited by the different muscle types and ages of the studies biopsies.

In summary, NMD plays a crucial role in regulating *NEB* transcripts in patients with pathogenic truncation variants, and a high incidence of cryptic splice site activation and intronic inclusion was found in patients with pathogenic splicing variants. Intronic inclusion was shown to lead to insertion of an unstructured sequence into actin binding motifs (Fig. 2b) and we propose that this disrupts the proper domain spacing actin binding sites on nebulin and that this negatively thin filament function. Considering that nebulin consists of a long chain of repeating units, each with thin filament binding sites that need to match with the regularly spaced thin filament proteins, the local displacement of a binding site is expected to have long range effects. Thus, a protein like nebulin might have heightened sensitivity to cryptic splice site activation. Additionally, our study underscored the importance of proper TFL, and that both shorter and longer than normal length can be detrimental. Finally, treatment with OM substantially increased force production in NEM2 patients, and the effect is largest for patients with the lowest level of nebulin. Given the absence of a curative treatment for NEM2, these results provide a foundation for future investigations into the potential therapeutic benefits of OM for NEM patients.

Supplementary Information The online version contains supplementary material available at https://doi.org/10.1007/s00401-024-02726-w.

Acknowledgements We are grateful to Shawn Granzier-Nakajima for developing dynamic stiffness software.

Funding This study was supported by the grant R01AR053897 from the National Institute of Arthritis and Musculoskeletal and Skin Disease.

Data availability Raw data were generated at the University of Arizona. Derived data supporting the findings of this study are available from the corresponding author on request.

Declarations

Conflict of interests The authors declare that they have no competing interests related to this study.

References

1. Anderson SL, Ekstein J, Donnelly MC, Keefe EM, Toto NR, LeVoci LA et al (2004) Nemaline myopathy in the Ashkenazi Jewish population is caused by a deletion in the nebulin gene. Hum Genet 115:185–190
2. Bang M-L, Gregorio C, Labeit S (2002) Molecular dissection of the interaction of desmin with the C-terminal region of nebulin. J Struct Biol 137:119–127
3. Bang M-L, Li X, Littlefield R, Bremner S, Thor A, Knowlton KU et al (2006) Nebulin-deficient mice exhibit shorter thin filament lengths and reduced contractile function in skeletal muscle. J Cell Biol 173:905–916
4. Brenner B (1986) The cross-bridge cycle in muscle. Mechanical, biochemical, and structural studies on single skinned rabbit psoas fibers to characterize cross-bridge kinetics in muscle for correlation with the actomyosin-ATPase in solution. Controversial issues in cardiac pathophysiology: Erwin Riesch Symposium, July 12/13, 1985. Springer, City, pp 1–15
5. Brogna S, Wen J (2009) Nonsense-mediated mRNA decay (NMD) mechanisms. Nat Struct Mol Biol 16:107–113
6. Campbell KB, Chandra M, Kirkpatrick RD, Slinker BK, Hunter WC (2004) Interpreting cardiac muscle force-length dynamics using a novel functional model. Am J Physiol Heart and Circ Physiol 286:H1535–H1545
7. Ceyhan-Birsoy O, Agrawal PB, Hidalgo C, Schmitz-Abe K, DeChene ET, Swanson LC et al (2013) Recessive truncating titin gene, TTN, mutations presenting as centronuclear myopathy. Neurology 81:1205–1214
8. Chandra M, Mamidi R, Ford S, Hidalgo C, Witt C, Ottenheijm C et al (2009) Nebulin alters cross-bridge cycling kinetics and increases thin filament activation: a novel mechanism for increasing tension and reducing tension cost. J Biol Chem 284:30889–30896
9. Chandra V, Gollapudi SK, Chandra M (2015) Rat cardiac troponin T mutation (F72L)-mediated impact on thin filament cooperativity is divergently modulated by α-and β-myosin heavy chain isoforms. Am J of Physiol Heart Circ Physiol 309:H1260–H1270
10. Conover GM, Henderson SN, Gregorio CC (2009) A myopathy-linked desmin mutation perturbs striated muscle actin filament architecture. Mol Biol Cell 20:834–845
11. Danecek P, Bonfield JK, Liddle J, Marshall J, Ohan V, Pollard MO, Whitwham A, Keane T, McCarthy SA, Davies RM (2021) Twelve years of SAMtools and BCFtools. Gigascience 10: giab008
12. de Sousa AR, Penalva LO, Marcotte EM, Vogel C (2009) Global signatures of protein and mRNA expression levels. Mol BioSyst 5:1512–1526
13. de Winter JM, Buck D, Hidalgo C, Jasper JR, Malik FI, Clarke NF et al (2013) Troponin activator augments muscle force in nemaline myopathy patients with nebulin mutations. J Med Genet 50:383–392
14. de Winter JM, Joureau B, Sequeira V, Clarke NF, van der Velden J, Stienen GJ et al (2015) Effect of levosimendan on the contractility of muscle fibers from nemaline myopathy patients with mutations in the nebulin gene. Skeletal muscle 5:1–10
15. de Winter JM, Molenaar JP, Yuen M, van der Pijl R, Shen S, Conijn S et al (2020) KBTBD13 is an actin-binding protein that modulates muscle kinetics. J Clin Invest 130:754–767. https://doi.org/10.1172/JCI124000
16. de Winter JM, Ottenheijm CAC (2017) Sarcomere dysfunction in nemaline myopathy. J Neuromuscul Dis 4:99–113. https://doi.org/10.3233/JND-160200
17. Dobin A, Davis CA, Schlesinger F, Drenkow J, Zaleski C, Jha S et al (2013) STAR: ultrafast universal RNA-seq aligner. Bioinformatics 29:15–21
18. Donkervoort S, Papadaki M, de Winter JM, Neu MB, Kirschner J, Bolduc V et al (2015) TPM3 deletions cause a hypercontractile congenital muscle stiffness phenotype. Ann Neurol 78:982–994. https://doi.org/10.1002/ana.24535
19. Donner K, Sandbacka M, Lehtokari V-L, Wallgren-Pettersson C, Pelin K (2004) Complete genomic structure of the human nebulin gene and identification of alternatively spliced transcripts. Eur J Hum Genet 12:744–751
20. Evans JM, Cox ML, Huska J, Li F, Gaitero L, Guo LT et al (2016) Exome sequencing reveals a nebulin nonsense mutation in a dog model of nemaline myopathy. Mamm Genome 27:495–502
21. Fabiato A, Fabiato F (1979) Calculator programs for computing the composition of the solutions containing multiple metals and ligands used for experiments in skinned muscle cells. J Physiol (Paris) 75:463–505
22. Fomin A, Gärtner A, Cyganek L, Tiburcy M, Tuleta I, Wellers L et al (2021) Truncated titin proteins and titin haploinsufficiency are targets for functional recovery in human cardiomyopathy due to TTN mutations. Science translational medicine 13:eabd3079
23. Ford SJ, Chandra M, Mamidi R, Dong W, Campbell KB (2010) Model representation of the nonlinear step response in cardiac muscle. J Gen Physiol 136:159–177
24. Fukuda N, Wu Y, Farman G, Irving TC, Granzier H (2005) Titin-based modulation of active tension and interfilament lattice spacing in skinned rat cardiac muscle. Pflugers Arch 449:449–457
25. Gohlke J, Tonino P, Lindqvist J, Smith JE III, Granzier H (2020) The number of Z-repeats and super-repeats in nebulin greatly

varies across vertebrates and scales with animal size. J Gen Physiol 153:e202012783
26. Gollapudi SK, Reda SM, Chandra M (2017) Omecamtiv mecarbil abolishes length-mediated increase in guinea pig cardiac myofiber Ca^{2+} sensitivity. Biophys J 113:880–888
27. Granzier HL, Akster HA, Ter Keurs HE (1991) Effect of thin filament length on the force-sarcomere length relation of skeletal muscle. Am J Physiol 260:C1060-1070. https://doi.org/10.1152/ajpcell.1991.260.5.C1060
28. Hinson JT, Chopra A, Nafissi N, Polacheck WJ, Benson CC, Swist S et al (2015) Titin mutations in iPS cells define sarcomere insufficiency as a cause of dilated cardiomyopathy. Science 349:982–986
29. Hoek TA, Khuperkar D, Lindeboom RG, Sonneveld S, Verhagen BM, Boersma S et al (2019) Single-molecule imaging uncovers rules governing nonsense-mediated mRNA decay. Mol Cell 75(324–339):e311
30. Kaplinsky E, Mallarkey G (2018) Cardiac myosin activators for heart failure therapy: focus on omecamtiv mecarbil. Drugs in context 7:212518
31. Kapustin Y, Chan E, Sarkar R, Wong F, Vorechovsky I, Winston RM et al (2011) Cryptic splice sites and split genes. Nucleic Acids Res 39:5837–5844
32. Kiiski K, Lehtokari V-L, Löytynoja A, Ahlstén L, Laitila J, Wallgren-Pettersson C et al (2016) A recurrent copy number variation of the NEB triplicate region: only revealed by the targeted nemaline myopathy CGH array. Eur J Hum Genet 24:574–580
33. Kiiski KJ, Lehtokari V-L, Vihola AK, Laitila JM, Huovinen S, Sagath LJ et al (2019) Dominantly inherited distal nemaline/cap myopathy caused by a large deletion in the nebulin gene. Neuromuscul Disord 29:97–107
34. Kim Y-g, Ha C, Shin S, Park J-h, Jang J-H, Kim J-W (2023) Enrichment of titin-truncating variants in exon 327 in dilated cardiomyopathy and its relevance to reduced nonsense-mediated mRNA decay efficiency. Front Genet 13:1087359
35. Kiss B, Gohlke J, Tonino P, Hourani Z, Kolb J, Strom J et al (2020) Nebulin and Lmod2 are critical for specifying thin-filament length in skeletal muscle. Sci Adv 6:eabc1992
36. Labeit S, Ottenheijm CA, Granzier H (2011) Nebulin, a major player in muscle health and disease. FASEB J 25:822–829
37. Lahmers S, Wu Y, Call DR, Labeit S, Granzier H (2004) Developmental control of titin isoform expression and passive stiffness in fetal and neonatal myocardium. Circ Res 94:505–513
38. Laitila J, Hanif M, Paetau A, Hujanen S, Keto J, Somervuo P et al (2012) Expression of multiple nebulin isoforms in human skeletal muscle and brain. Muscle Nerve 46:730–737
39. Lawlor MW, Ottenheijm CA, Lehtokari V-L, Cho K, Pelin K, Wallgren-Pettersson C et al (2011) Novel mutations in NEB cause abnormal nebulin expression and markedly impaired muscle force generation in severe nemaline myopathy. Skeletal muscle 1:1–12
40. Le Hir H, Gatfield D, Izaurralde E, Moore MJ (2001) The exon–exon junction complex provides a binding platform for factors involved in mRNA export and nonsense-mediated mRNA decay. EMBO J 20:4987–4997
41. Lehtokari VL, Kiiski K, Sandaradura SA, Laporte J, Repo P, Frey JA et al (2014) Mutation update: the spectra of nebulin variants and associated myopathies. Hum Mutat 35:1418–1426
42. Li F, Buck D, De Winter J, Kolb J, Meng H, Birch C et al (2015) Nebulin deficiency in adult muscle causes sarcomere defects and muscle-type-dependent changes in trophicity: novel insights in nemaline myopathy. Hum Mol Genet 24:5219–5233
43. Linde L, Boelz S, Neu-Yilik G, Kulozik AE, Kerem B (2007) The efficiency of nonsense-mediated mRNA decay is an inherent character and varies among different cells. Eur J Hum Genet 15:1156–1162
44. Lindeboom RG, Supek F, Lehner B (2016) The rules and impact of nonsense-mediated mRNA decay in human cancers. Nat Genet 48:1112–1118
45. Lindeboom RG, Vermeulen M, Lehner B, Supek F (2019) The impact of nonsense-mediated mRNA decay on genetic disease, gene editing and cancer immunotherapy. Nat Genet 51:1645–1651
46. Lindqvist J, Granzier H (2023) Pharmacological Inhibition of myostatin in a mouse model of typical nemaline myopathy increases muscle size and force. Int J Mol Sci 24:15124
47. Lindqvist J, Lee E-J, Karimi E, Kolb J, Granzier H (2019) Omecamtiv mecarbil lowers the contractile deficit in a mouse model of nebulin-based nemaline myopathy. PLoS ONE 14:e0224467
48. Lindqvist J, Ma W, Li F, Hernandez Y, Kolb J, Kiss B et al (2020) Triggering typical nemaline myopathy with compound heterozygous nebulin mutations reveals myofilament structural changes as pathomechanism. Nat Commun 11:2699
49. Malik FI, Hartman JJ, Elias KA, Morgan BP, Rodriguez H, Brejc K et al (2011) Cardiac myosin activation: a potential therapeutic approach for systolic heart failure. Science 331:1439–1443
50. Mancini E, Iserte J, Yanovsky M, Chernomoretz A (2019) ASpli: Analysis of alternative splicing using RNA-Seq. R package version 1
51. Methawasin M, Farman GP, Granzier-Nakajima S, Strom J, Kiss B, Smith JE III et al (2022) Shortening the thick filament by partial deletion of titin's C-zone alters cardiac function by reducing the operating sarcomere length range. J Mol Cell Cardiol 165:103–114
52. Mirdita M, Schütze K, Moriwaki Y, Heo L, Ovchinnikov S, Steinegger M (2022) ColabFold: making protein folding accessible to all. Nat Methods 19:679–682
53. Moreau-Le Lan S, Aller E, Calabria I, Gonzalez-Tarancon L, Cardona-Gay C, Martinez-Matilla M et al (2018) New mutations found by next-generation sequencing screening of spanish patients with nemaline myopathy. PLoS ONE 13:e0207296
54. Nagy E, Maquat LE (1998) A rule for termination-codon position within intron-containing genes: when nonsense affects RNA abundance. Trends Biochem Sci 23:198–199
55. Nagy L, Kovács Á, Bódi B, Pásztor E, Fülöp GÁ, Tóth A et al (2015) The novel cardiac myosin activator omecamtiv mecarbil increases the calcium sensitivity of force production in isolated cardiomyocytes and skeletal muscle fibres of the rat. Br J Pharmacol 172:4506–4518
56. Neuhaus SB, Wallgren-Pettersson C, Bönnemann CG, Schara U, Servais L (2020) 250th ENMC International Workshop: Clinical trial readiness in nemaline myopathy 6–8 September 2019, Hoofdorp, the Netherlands.
57. North K, Laing NG, Wallgren-Pettersson C (1997) Nemaline myopathy: current concepts. The ENMC international consortium and nemaline myopathy. J Med Genet 34:705
58. Ochala J, Lehtokari V-L, Iwamoto H, Li M, Feng H-Z, Jin J-P et al (2011) Disrupted myosin cross-bridge cycling kinetics triggers muscle weakness in nebulin-related myopathy. FASEB J 25:1903
59. Ottenheijm C, Granzier H, Labeit S (2012) The sarcomeric protein nebulin: another multifunctional giant in charge of muscle strength optimization. Front Physiol 3:37
60. Ottenheijm CA, Buck D, de Winter JM, Ferrara C, Piroddi N, Tesi C et al (2013) Deleting exon 55 from the nebulin gene induces severe muscle weakness in a mouse model for nemaline myopathy. Brain 136:1718–1731
61. Ottenheijm CA, Hooijman P, DeChene ET, Stienen GJ, Beggs AH, Granzier H (2010) Altered myofilament function depresses force generation in patients with nebulin-based nemaline myopathy (NEM2). J Struct Biol 170:334–343

62. Ottenheijm CA, Witt CC, Stienen GJ, Labeit S, Beggs AH, Granzier H (2009) Thin filament length dysregulation contributes to muscle weakness in nemaline myopathy patients with nebulin deficiency. Hum Mol Genet 18:2359–2369
63. Pappas CT, Bhattacharya N, Cooper JA, Gregorio CC (2008) Nebulin interacts with CapZ and regulates thin filament architecture within the Z-disc. Mol Biol Cell 19:1837–1847
64. Pelin K, Wallgren-Pettersson C (2008) Nebulin—a giant chameleon. The sarcomere and skeletal muscle disease. Springer, City, pp 28–39
65. Pellegrino J, Ruby BC, Dumke CL (2016) Effect of plyometrics on the energy cost of running and MHC and titin isoforms. Med Sci Sports Exerc 48:49–56
66. Psotka MA, Teerlink JR (2017) Direct myosin activation by omecamtiv mecarbil for heart failure with reduced ejection fraction. Heart Failure 247(465):490
67. Reda SM, Gollapudi SK, Chandra M (2016) L71F mutation in rat cardiac troponin T augments crossbridge recruitment and detachment dynamics against α-myosin heavy chain, but not against β-myosin heavy chain. J Muscle Res Cell Motil 37:215–223
68. Reed UC, Marie SK, Zanoteli E, Fireman MA, Oliveira AS, Werneck LC et al (2003) Rod distribution and muscle fiber type modification in the progression of nemaline myopathy. J Child Neurol 18:235–240
69. Roberts AM, Ware JS, Herman DS, Schafer S, Baksi J, Bick AG et al (2015) Integrated allelic, transcriptional, and phenomic dissection of the cardiac effects of titin truncations in health and disease. Sci Trans Med 7:270ra276
70. Roca X, Sachidanandam R, Krainer AR (2003) Intrinsic differences between authentic and cryptic 5′ splice sites. Nucleic Acids Res 31:6321–6333
71. Romero NB, Sandaradura SA, Clarke NF (2013) Recent advances in nemaline myopathy. Curr Opin Neurol 26:519–526
72. Ryan MM, Schnell C, Strickland CD, Shield LK, Morgan G, Iannaccone ST et al (2001) Nemaline myopathy: a clinical study of 143 cases. Ann Neurol Off J Am Neurol Assoc Child Neurol Soc 50:312–320
73. Sanoudou D, Beggs AH (2001) Clinical and genetic heterogeneity in nemaline myopathy–a disease of skeletal muscle thin filaments. Trends Mol Med 7:362–368
74. Schafer S, De Marvao A, Adami E, Fiedler LR, Ng B, Khin E et al (2017) Titin-truncating variants affect heart function in disease cohorts and the general population. Nat Genet 49:46–53
75. Schiaffino S, Reggiani C (2011) Fiber types in mammalian skeletal muscles. Physiol Rev 91:1447–1531
76. Schiaffino S, Reggiani C (1996) Molecular diversity of myofibrillar proteins: gene regulation and functional significance. Physiol Rev 76:371–423
77. Sewry CA, Laitila JM, Wallgren-Pettersson C (2019) Nemaline myopathies: a current view. J Muscle Res Cell Motil 40:111–126. https://doi.org/10.1007/s10974-019-09519-9
78. Singh NN, Del Rio-Malewski JB, Luo D, Ottesen EW, Howell MD, Singh RN (2017) Activation of a cryptic 5′ splice site reverses the impact of pathogenic splice site mutations in the spinal muscular atrophy gene. Nucleic Acids Res 45:12214–12240
79. Sun Y-B, Irving M (2010) The molecular basis of the steep force–calcium relation in heart muscle. J Mol Cell Cardiol 48:859–865
80. Sztal TE, McKaige EA, Williams C, Oorschot V, Ramm G, Bryson-Richardson RJ (2018) Testing of therapies in a novel nebulin nemaline myopathy model demonstrate a lack of efficacy. Acta Neuropathol Commun 6:1–10
81. Teerlink JR, Clarke CP, Saikali KG, Lee JH, Chen MM, Escandon RD et al (2011) Dose-dependent augmentation of cardiac systolic function with the selective cardiac myosin activator, omecamtiv mecarbil: a first-in-man study. The Lancet 378:667–675
82. Telfer WR, Nelson DD, Waugh T, Brooks SV, Dowling JJ (2012) Neb: a zebrafish model of nemaline myopathy due to nebulin mutation. Dis Model Mech 5:389–396. https://doi.org/10.1242/dmm.008631
83. Tinklenberg JA, Siebers EM, Beatka MJ, Fickau BA, Ayres S, Meng H et al (2019) Myostatin inhibition using ActRIIB-mFc does not produce weight gain or strength in the nebulin conditional KO mouse. J Neuropathol Exp Neurol 78:130–139
84. Tinklenberg JA, Siebers EM, Beatka MJ, Meng H, Yang L, Zhang Z et al (2017) Myostatin inhibition using mRK35 produces skeletal muscle growth and tubular aggregate formation in wild type and Tg ACTA1 D286G nemaline myopathy mice. Hum Mol Genet 27:638–648
85. Tirrell TF, Cook MS, Carr JA, Lin E, Ward SR, Lieber RL (2012) Human skeletal muscle biochemical diversity. J Exp Biol 215:2551–2559
86. Tonino P, Pappas CT, Hudson BD, Labeit S, Gregorio CC, Granzier H (2010) Reduced myofibrillar connectivity and increased Z-disk width in nebulin-deficient skeletal muscle. J Cell Sci 123:384–391
87. van de Locht M, Borsboom TC, Winter JM, Ottenheijm CAC (2021) Troponin variants in congenital myopathies: how they affect skeletal muscle mechanics. Int J Mol Sci 22:9187. https://doi.org/10.3390/ijms22179187
88. van Heesch S, Witte F, Schneider-Lunitz V, Schulz JF, Adami E, Faber AB et al (2019) The translational landscape of the human heart. Cell 178(242–260):e229
89. Vogel C, Marcotte EM (2012) Insights into the regulation of protein abundance from proteomic and transcriptomic analyses. Nat Rev Genet 13:227–232
90. Wallgren-Pettersson C, Donner K, Sewry C, Bijlsma E, Lammens M, Bushby K et al (2002) Mutations in the nebulin gene can cause severe congenital nemaline myopathy. Neuromuscul Disord 12:674–679
91. Wallgren-Pettersson C, Laing NG (2000) Report of the 70th ENMC international workshop: nemaline myopathy, 11–13 June 1999, Naarden, the Netherlands. Neuromuscul Disord 10:299–306
92. Wallgren-Pettersson C, Laing NG (2001) Report of the 83rd ENMC international workshop: 4th workshop on nemaline myopathy, 22–24 September 2000, Naarden, the Netherlands. Neuromuscul Disord 11:589–595
93. Wallgren-Pettersson C, Lehtokari V-L, Kalimo H, Paetau A, Nuutinen E, Hackman P et al (2007) Distal myopathy caused by homozygous missense mutations in the nebulin gene. Brain 130:1465–1476
94. Wallgren-Pettersson C, Pelin K, Hilpelä P, Donner K, Porfirio B, Graziano C et al (1999) Clinical and genetic heterogeneity in autosomal recessive nemaline myopathy. Neuromuscul Disord 9:564–572
95. Wallgren-Pettersson C, Sewry CA, Nowak KJ, Laing NG (2011) Nemaline myopathies. Seminars in pediatric neurology. Elsevier, City, pp 230–238
96. Wang Z, Grange M, Pospich S, Wagner T, Kho AL, Gautel M et al (2022) Structures from intact myofibrils reveal mechanism of thin filament regulation through nebulin. Science 375:eabn1934
97. Warren CM, Greaser ML (2003) Method for cardiac myosin heavy chain separation by sodium dodecyl sulfate gel electrophoresis. Anal Biochem 320:149–151
98. Warren CM, Jordan MC, Roos KP, Krzesinski PR, Greaser ML (2003) Titin isoform expression in normal and hypertensive myocardium. Cardiovasc Res 59:86–94
99. Warren CM, Krzesinski PR, Greaser ML (2003) Vertical agarose gel electrophoresis and electroblotting of high-molecular-weight proteins. Electrophoresis 24:1695–1702

100. Winter JM, Joureau B, Lee EJ, Kiss B, Yuen M, Gupta VA et al (2016) Mutation-specific effects on thin filament length in thin filament myopathy. Ann Neurol 79:959–969. https://doi.org/10.1002/ana.24654
101. Winter JMd, Joureau B, Lee EJ, Kiss B, Yuen M, Gupta VA et al (2016) Mutation-specific effects on thin filament length in thin filament myopathy. Ann Neurol 79:959–969
102. Witt CC, Burkart C, Labeit D, McNabb M, Wu Y, Granzier H et al (2006) Nebulin regulates thin filament length, contractility, and Z-disk structure in vivo. EMBO J 25:3843–3855
103. Woody MS, Greenberg MJ, Barua B, Winkelmann DA, Goldman YE, Ostap EM (2018) Positive cardiac inotrope omecamtiv mecarbil activates muscle despite suppressing the myosin working stroke. Nat Commun 9:1–11
104. Yuen M, Ottenheijm CA (2020) Nebulin: big protein with big responsibilities. J Muscle Res Cell Motil 41:103–124
105. Yuen M, Sandaradura SA, Dowling JJ, Kostyukova AS, Moroz N, Quinlan KG et al (2014) Leiomodin-3 dysfunction results in thin filament disorganization and nemaline myopathy. J Clin Invest 124:4693–4708. https://doi.org/10.1172/JCI75199
106. Zetoune AB, Fontanière S, Magnin D, Anczuków O, Buisson M, Zhang CX et al (2008) Comparison of nonsense-mediated mRNA decay efficiency in various murine tissues. BMC Genet 9:1–11